Methodological Aspects of Clinical fMRI - Reliability Assessment and Development of Data Analysis Strategies

Mannfolk, Peter

2010

Methodological Aspects of Clinical fMRI

Reliability Assessment and Development of Data Analysis Strategies

Peter Mannfolk

Department of Medical Radiation Physics

Clinical Sciences, Lund

Lund University, Sweden

Thesis for the Degree of Doctor of Philosophy
Faculty of Science, Lund University
Department of Medical Radiation Physics
Clinical Sciences, Lund
Skåne University Hospital, Lund
SE-221 85 Lund, Sweden

ISBN 978-91-86671-99-0
Printed in Sweden by Media-Tryck, Lund 2010

I may not have gone where I intended to go,
but I think I have ended up where I needed to be
- Douglas Adams

Abstract

Functional magnetic resonance imaging (fMRI) is a non-invasive technique used for the investigation of brain function, which has found numerous applications within basic neuroscience. The introduction of fMRI as a clinical tool for presurgical mapping of pertinent cortical regions in patients with tumour or epilepsy has facilitated neurosurgical planning, and most likely reduced the risk of severe postoperative deficits. However, there is a fundamental difference between the application of fMRI in experimental research and in the clinical setting. While inference is often drawn from data on group level in neuroscientific applications of fMRI, the clinical use of the method demands that reliable results be obtained in individual patients.

The aims of the methodological studies presented in this thesis were to increase the reliability and extend the usefulness of clinical fMRI. In one study, gradient-echo field maps were utilized to assess the sensitivity of echo-planar imaging to the blood oxygenation level dependent (BOLD) contrast. Theoretical expressions for the calculation of the BOLD sensitivity were verified and improved. The BOLD sensitivity was investigated in a group of healthy volunteers using a clinical magnetic resonance imaging (MRI) system, and it was concluded that the field map method accurately predicts BOLD sensitivity. In another study, a flexible model was introduced in order to increase the confidence of clinical fMRI examinations of patients unable to fully comply with a typical clinical fMRI experiment. The method was applied to experimental and simulated data, and then used to retrospectively analyse patient data. The conclusion drawn from this study was that the proposed flexible model improves the detection of activation in partially non-compliant subjects. In the third study included in this thesis, the model-free algorithm locally linear embedding was applied to fMRI data analysis. The proposed data-driven algorithm was optimized and investigated with respect to reliability and possible benefits in a clinical setting. The algorithm was found to compare well to the traditionally used method of principal component analysis, and showed benefits when applied to simulated fMRI data exhibiting non-linear characteristics. Finally, the test-retest reliability of resting-state fMRI was compared with the reliability of traditional task-based fMRI. Resting-state fMRI compared well with task-based fMRI experiments, thus possibly extending the use of fMRI to patient groups that have hitherto not been able to benefit from fMRI examinations.

Original papers

This thesis is based on studies reported in the following papers, referred to in the text by their Roman numerals. Published papers are reprinted by kind permission of the copyright owners.

I Mannfolk P, Wirestam R, Nilsson M, van Westen D, Ståhlberg F, Olsrud J
Assessment of spatial BOLD sensitivity variations in fMRI using gradient-echo field maps.
Magnetic Resonance Imaging 2010;28(7):947-56

II Waites AB, Mannfolk P, Shaw ME, Olsrud J, Jackson GD
Flexible statistical modelling detects clinical functional magnetic resonance imaging activation in partially compliant subjects.
Magnetic Resonance Imaging 2007;25(2):188-96

III Mannfolk P, Wirestam R, Nilsson M, Ståhlberg F, Olsrud J
Dimensionality reduction of fMRI time series data using locally linear embedding.
Magnetic Resonance Materials in Physics, Biology and Medicine 2010
Epublished ahead of print, March 13. DOI 10.1007/s10334-010-0204-0

IV Mannfolk P, Nilsson M, Hansson H, Ståhlberg F, Fransson P, Weibull A, Svensson J, Wirestam R, Olsrud J
Can resting state fMRI serve as a complement to task-evoked mapping of sensorimotor function? A test-retest reliability study in healthy volunteers.
Submitted to Journal of Magnetic Resonance Imaging

Abbreviations

BOLD	Blood oxygenation level dependent
CBF	Cerebral blood flow
CBV	Cerebral blood volume
EPI	Echo-planar imaging
fMRI	Functional magnetic resonance imaging
GLM	General linear model
HRF	Hemodynamic response function
ICA	Independent component analysis
LLE	Locally linear embedding
MDS	Multi-dimensional scaling
MRI	Magnetic resonance imaging
PCA	Principal component analysis
RF	Radio frequency
ROC	Receiver operating characteristic
SNR	Signal-to-noise ratio
TC	Nominal echo time
TE	Effective echo time
TR	Repetition time

Contents

1. Introduction

Since its introduction in the early 1990s, functional magnetic resonance imaging (fMRI) has become a successful non-invasive tool for probing the functional architecture of the brain. The study of the physiology that governs the contrast utilized in fMRI has, however, a much longer history. In 1890, Roy and Sherrington (1) discovered that the regulation of blood flow and blood oxygenation in the brain were closely coupled to neuronal activity. They observed that stimulation of specific regions of the brain increased the blood flow in these areas and, furthermore, that the amount of oxygen extracted from the blood was smaller than the amount delivered. A study by Pauling and Coryell in 1936 (2), established that the oxygen bound to haemoglobin is diamagnetic, whereas deoxygenated haemoglobin is paramagnetic. The magnetic properties of deoxy-haemoglobin and oxyhaemoglobin were further studied by Thulborn et al. who, in 1982, observed the dependence of the transverse relaxation rate of water protons on the blood oxygenation level (3). The local increase in oxygen concentration in the blood resulting from the stimulation of various regions of the brain is the physiological foundation of the so-called blood oxygenation level dependent (BOLD) contrast that is utilized in fMRI (4,5). The BOLD contrast was, however, not utilized for studies of brain activation until the early 1990s, when several research groups investigated this application (6-10).

1.1 Applications of fMRI

The initial applications of fMRI focused on the localization of various cerebral functions, including the mapping of functional areas in the brain responsible for motor control, sensory input, language and memory (6,8,11,12). These applications have primarily been investigated by the use of prolonged blocks of stimuli interleaved with some baseline condition (often represented by the subject being at rest). With the introduction of higher magnetic field strengths and more sophisticated analysis strategies, the investigation of the actual haemodynamic response to a single stimulus was made possible. This also promoted the application of other types of paradigms allowing the registration of subject response to an individual stimulus. The use of more elaborate paradigms has further allowed investigations of phenomena such as learning and attention (13,14). A subject of great interest to the neuroscientific community is the establishment of functionally

connected networks, first demonstrated by Biswal et al., in 1995 (15). Such networks, exhibiting correlating changes in brain activation, exist both during task and in varied states of consciousness. The study of resting-state activation, i.e., spontaneous signal fluctuations observed in subjects at rest or asleep is an important aspect of functional connectivity analysis. A number of reproducible networks have been established, and the study of these networks may lead to a deeper understanding of the brain, as well as possible clinical applications (16).

1.2 Clinical use of fMRI

The reliability of BOLD fMRI has improved with the advent of robust paradigms, new data analysis methods and hardware development, facilitating the introduction of the method into the clinical environment. An important clinical application is the mapping of functional areas of the brain at risk prior to surgical resection of tumours, and of parts of the brain inflicting epileptic seizures (17-23). BOLD fMRI has evolved into a complementary method for such procedures, replacing invasive methods such as electrocortical stimulation (24) and the Wada test (25).

An important aspect of fMRI in general and of the clinical implementation of fMRI in particular, is the sensitivity of the method. A method to be used as a tool for presurgical mapping must perform well with respect to the detection of truly activated brain areas, otherwise the risk of a surgical resection of pertinent areas at risk will increase. While fMRI generally has been shown to exhibit good sensitivity, methodological limitations exist that potentially prevent truly activated areas of the brain to be detected. Such limitations arise from both the fMRI data acquisition and the subsequent data analysis. Furthermore, the design and analysis of the clinical fMRI experiment has, so far, restricted fMRI to patient groups able to fully comply with a given task. Hence, noncompliant patient groups, such as children or patients with certain cognitive or physiological deficits, cannot reliably be presurgically assessed using fMRI. It is of importance to address such methodological issues in order to increase the confidence in the fMRI results as well as to extend the range of clinical fMRI applications.

1.3 Aims

The aims of the research projects reported in this thesis were to investigate and optimize methodological aspects of importance for the use of BOLD fMRI as a clinical tool.

Specifically, a method for quantification of BOLD sensitivity by the use of field maps has been validated and improved (Paper I). Furthermore, the BOLD sensitivity was assessed for a group of healthy volunteers in order to characterize a clinical magnetic resonance imaging (MRI) system. The dependence of BOLD sensitivity on subject motion and head positioning was also addressed. In an effort to increase the sensitivity of clinical fMRI in partially non-compliant patients, a flexible model was developed and validated with respect to its performance in identifying relevant activation (Paper II). Furthermore, a non-linear dimensionality reduction algorithm was introduced and characterized in terms of reliability and possible benefits in a clinical setting (Paper III). In order to further extend the clinical use of fMRI, the method of resting state fMRI was investigated with respect to test-retest reliability (Paper IV). Measurements of resting-state activation of the motor network were evaluated in a group of healthy volunteers and compared with the corresponding results from a traditional task-based experiment.

2. Concepts of BOLD fMRI

The contrast mechanism utilized in BOLD fMRI is based on the local oxygenation level of the cerebral blood. In this chapter, the physiology of the BOLD phenomenon is described, as well as the way in which an fMRI experiment is conducted with respect to the choice of pulse sequence and appropriate imaging parameters.

2.1 The physiology of the BOLD contrast

2.1.1 Origin of the BOLD contrast

The BOLD effect on the MRI signal results from the fact that the magnetic susceptibility of blood is dependent on its oxygenation state. The magnetic susceptibility describes how a material is magnetized by an applied magnetic field, and the induced magnetization results in geometry-dependent distortion of the magnetic field lines in and around the material. The distortion of the magnetic field lines depends on the magnetic susceptibility and shape of the magnetized material. Hence, the induced magnetic field increases and decreases the applied field in paramagnetic and diamagnetic materials, respectively.

Normal blood can exhibit both paramagnetic and diamagnetic properties depending on its oxygenation state. When oxygen is bound to the haemoglobin it is diamagnetic, while deoxygenated haemoglobin is paramagnetic (2). The effects of the blood oxygenation level on the transverse relaxation rate were investigated by Thulborn et al. (3). They concluded that oxygenation-state-dependent changes in the transverse relaxation rate, R2, were due to the diffusion of water molecules through magnetic field gradients caused by differences in susceptibility within the intravascular space. The magnetic field gradient, occurring as deoxygenation of the blood increases, will thus decrease T2 of the blood. The magnetic field gradients, however, extend into the surrounding tissue, which leads to a change in tissue T2* as well. This extravascular perturbation effect on the T2* relaxation rate, arising from the increased intravascular susceptibility, was observed by Ogawa et al. using gradient-echo images of a rat brain during hypoxia (5). The authors suggested that this effect could be used to image effects related to neuronal activation.

In a typical BOLD fMRI experiment, an increase in the signal is seen as a result of neuronal activation, which indicates that the oxygenation state of the blood has been altered. In order to understand this change in oxygenation state, the mechanisms of neuronal activation must be considered. In a simple description, a neuron consists of the soma (the cell body), dendrites and an axon (Fig. 2.1). The dendrites and the axon are filaments extending from the soma. The dendrites branch as they extend from the soma, normally over a few micrometres, whereas the axon can extend as far as a metre, branching several hundred times. Neuronal activation is the process of signalling between neurons, where signals flow from the axon of one neuron to the dendrites or the soma of another neuron. The interface between the termination of an axon (the axon terminal) and a dendrite or soma is called the synapse, which is the junction between the signalling neuron and the receiving dendrite or soma. Electrical or chemical signals are then transmitted from the membrane of the axon to the membrane of the dendrite or soma. This signalling process is used by a number of specialized neurons, for example, sensory and motor neurons, in order to facilitate sensory input to the central nervous system or to cause muscle contraction.

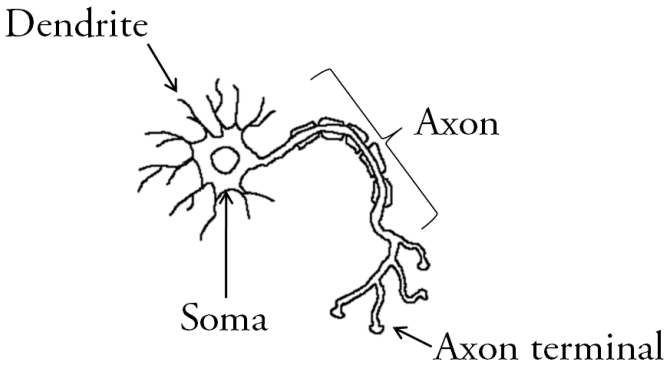

Figure 2.1. Schematic illustration of a neuron.

Neuronal activation increases the demand for energy, requiring more glucose and oxygen to be delivered. The observed increase in BOLD signal following neuronal activation may thus appear to be counterintuitive if one assumes that neuronal activation implies an increase in oxygen demand, leading to deoxygenation of the blood and thus a decrease in the signal due to shortening of the T2* of tissue. However, as observed by Fox et al. (26,27), neuronal activation leads to an increase in cerebral blood flow (CBF) that considerably overcompensates the increased oxygen demand by an excess supply of oxygenated blood. This mechanism leads to

a decrease in the magnetic field gradient as the diamagnetic properties of oxygenated blood are more similar to those of the surrounding tissue, thus leading to an increase in the signal due to an increase in T2* of the tissue.

2.1.2 Temporal characteristics of the haemodynamic response

The time course of the BOLD response to a brief stimulus is called the haemodynamic response function (HRF). The HRF is characterized by an initial dip, approximately 0.5-1 s after the stimulus onset, as observed by Menon et al. (28). This dip corresponds to a decrease in the signal below the baseline level (≈0.5%), and reflects an initial increase in the cerebral metabolic rate of oxygen in response to the onset of stimulation (29,30). In a study on BOLD dynamics, Buxton et al. developed the so-called balloon model (31), extending the work carried out by Davis et al. (29), where the initial dip is explained by an initial rapid increase in both CBF and the cerebral blood volume (CBV). In this initial phase, deoxyhaemoglobin increases due to the increased CBV. Due to a slight latency in the circulatory response, the signal increases after 5-8 s (the positive BOLD response) as CBF increases, reaching a maximum. The balloon model states that the volume in this phase increases more slowly than the flow, which leads to the positive BOLD overshoot, since CBF reaches its steady-state level before the CBV. As the CBV eventually reaches steady state, increasing the amount of deoxyhaemoglobin, the BOLD signal decreases to a steady-state level in the case of sustained stimulus, lasting until its cessation. The amplitudes of both the initial dip and the positive response are dependent on the external magnetic field strength (4). The signal then decreases, returning to the baseline level. This phase is often accompanied by a so-called post-stimulus undershoot, during which the signal passes below the baseline, remaining negative for several seconds, before finally returning to the baseline. This is also explained by the CBV decreasing more slowly than the CBF, leading to an elevated amount of deoxyhaemoglobin, and consequently a lower BOLD signal (Fig. 2.2). It should be noted that although the haemodynamic response function following a brief stimulation has been found to be relatively invariant (32), the corresponding response to sustained stimulation is somewhat variable (33). The overshoot and undershoot are not always present, and their magnitudes, when present, are highly variable. Furthermore, a delay in the haemodynamic response has been observed in stroke patients (34) and in tumour patients (35).

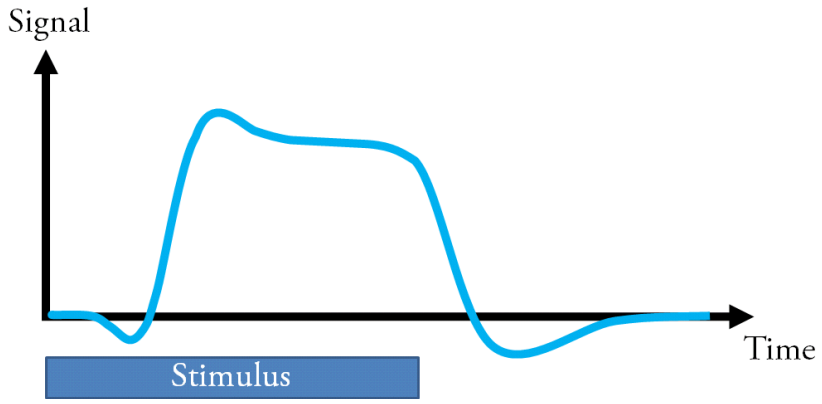

Figure 2.2. The haemodynamic response to sustained stimulus.

2.2 The fMRI experiment

The BOLD contrast normally yields a signal difference of only a few percent between the baseline state and the activation task. This emphasizes the need for the collection of multiple data in time, in order to be able to separate the two states statistically. Therefore, an fMRI experiment normally employs some kind of paradigm, i.e., a scheme defining when one or several specific task(s) should be performed during the course of the experiment. The simplest paradigm is the so-called block paradigm, consisting of alternating task and baseline conditions; the length of each block being typically 15-30 s. Normally, four or five blocks are used, which, for a repetition time (TR) of 2-3 s yields 50-150 volumes of gradient-echo echo-planar imaging (EPI) data acquired during 2-5 minutes. This type of paradigm is robust and normally employed clinically. For example, finger-tapping and foot movement paradigms are used for mapping the motor cortex. Word generation tasks are also important clinical paradigms when mapping and lateralizing the language areas.

However, investigators often try to detect the response to individual events. This could be due to the nature of the task, which, for example, could be determined at run-time or after the actual experiment. The investigator may, for instance, be interested in events occurring only at times when the subject responded in a certain way. An example is when the subject is asked a question, which the investigator then will treat differently depending on if the subject gave the correct answer or the wrong answer. This type of paradigm is called an event-related paradigm, and

offers greater flexibility. However, the small change in BOLD signal following a single stimulus means that an event-related paradigm must be averaged over multiple samples of the HRF in order to increase the statistical power, leading to longer experiments.

2.3 Pulse sequences

2.3.1 Gradient-echo techniques

The initial observations of the BOLD effect by Ogawa et al. (4) were made using the T2*-weighted 2D gradient-echo pulse sequence originally proposed by Haase et al. (36) under the acronym FLASH (Fast Low-Angle Shot). This pulse sequence was also used in other early studies for the detection of functional activation of the human brain (7,37,38). When applied to fMRI, the FLASH sequence requires an acquisition time of several seconds for a rather limited number of slices. This significantly limits the spatial coverage at a temporal resolution sufficient to allow dynamic monitoring of the BOLD contrast. An extension of the FLASH sequence was proposed by Menon et al. (39), in which the polarity of the readout gradient was reversed in order to form multiple echoes following a single radio frequency (RF) excitation pulse. By applying the same phase-encoding gradient to all echoes, multiple images can be acquired, reflecting the decay of transverse magnetization, allowing T2* to be calculated on a pixel-by-pixel basis.

In order to address the problem of long acquisition times, multiple echoes following a single RF excitation pulse can also be utilized for rapid image acquisition. By applying different phase-encoding gradients to each echo, the *k*-space can be filled very rapidly, thereby providing a means of acquiring multiple slices with high temporal resolution. This concept was first introduced by Mansfield (40), who proposed the EPI readout technique. In the original formulation of the EPI pulse sequence, a constant phase-encoding gradient was applied, whereas the dominating EPI pulse sequence of today utilizes the *k*-space traversal scheme proposed by Johnson et al. (41), according to which the whole *k*-space is sampled in a rectilinear fashion using a blipped phase-encoding gradient. In a study by Turner et al. (10), the EPI technique was applied to monitor rapid changes in blood oxygenation of the cat brain. The first reported human fMRI experiments followed shortly, in which visual stimulation paradigms were used to assess neuronal activation of the primary visual cortex. This was performed by utilizing the BOLD contrast (8,9), and measurements of the changes in CBV using a gadolinium-based paramagnetic contrast agent (42). Other early studies on

human BOLD fMRI successfully employed motor activation paradigms (6,8). Although the rectilinear *k*-space traversal strategy is the dominant strategy, spiral EPI has also been used for fMRI (43).

The EPI technique offers very rapid imaging due to the use of a single excitation RF pulse, allowing acquisition times as short as 50-70 ms for a single slice. Using a TR of 2-3 s, full brain coverage can be obtained. Furthermore, when using a repetition time of several seconds, the pulse sequence is relatively insensitive to inflow effects, i.e., full longitudinal relaxation of the excited spins makes the effect of inflowing spins negligible (44).

The EPI sequence is, however, sensitive to off-resonance effects, due to the low bandwidth in the phase-encoding direction. This implies that chemical shift artefacts are substantial in EPI, approaching several centimetres. However, this type of artefact can be effectively suppressed by using different types of fat-saturation techniques. The low bandwidth in the phase-encoding direction also creates geometric image distortion and signal loss in areas exhibiting magnetic field inhomogeneities arising from interfaces between materials with different magnetic susceptibilities (e.g., brain and air). Distortion corrections can be performed by measuring the local magnetic field in the object using so-called field maps (45). However, signal loss due to magnetic field inhomogeneities cannot be recovered. The introduction of parallel imaging techniques, using the individual sensitivity profiles from multiple coils, shortens the readout time, thereby reducing the effects of off-resonance conditions. Several different approaches to implementing this general strategy have been proposed, including sensitivity encoding (46) and simultaneous acquisition of spatial harmonics (47).

Furthermore, the switching of the gradients during a pulse sequence results in the induction of eddy currents in the conducting surfaces of the MRI system. This phenomenon is present in all types of MRI pulse sequences, but is more pronounced in EPI due to the rapid switching of the gradients and the longer total readout time. The eddy currents lead to magnetic field gradients which, in turn, create time-dependent frequency shifts. The frequency shifts correspond to phase differences between the lines in the raw data, resulting from the alternating gradient polarity used in EPI, which ultimately manifest themselves as ghost images in the magnitude EPI image. Strategies for the suppression of these eddy current effects include effective coil design, minimizing eddy current induction, as well as adjustment of the phase information after data acquisition. The third strategy can be implemented by measuring the phase shifts in a reference data set,

which can subsequently be used to correct the raw EPI data (48). The correction can also be performed by measuring the phase shifts in the actual EPI data, as proposed by Buonocore & Gao (49). Furthermore, physiological sources such as respiratory- or cardiac-induced phase variations or subject motion, can significantly affect the stability of the signal when using pulse sequences with multiple excitations. These effects can be minimized by the use of so-called navigator echoes (50). Data acquisition can also be gated using hardware in order to minimize the influence of respiratory- or cardiac-induced signal variations. This can, however, lead to variations in TR, which in turn affect the longitudinal magnetization recovery, and hence the signal stability over time, and gating methods are therefore rarely used in fMRI experiments.

2.3.2 Spin-echo techniques

The 180° refocusing RF pulse utilized by a spin-echo pulse sequence will remove the dephasing effects of macroscopic, time-invariant magnetic field inhomogeneities, but will also reduce the effects of microscopic inhomogeneities arising from the BOLD effect. Thus, a spin-echo pulse sequence, although suffering less signal loss, will exhibit a smaller BOLD effect than the gradient-echo sequence. In particular, the extravascular component of the BOLD signal will be reduced. The intravascular BOLD signal will, however, be retained, thus providing better localization of the BOLD effect.

Spin-echo EPI employs a single 180° refocusing pulse followed by the same traversal of *k*-space as described above for the gradient-echo EPI. The pulse sequence is arranged so that the centre of *k*-space is covered at the time of the centre of the spin echo. As explained above, extravascular BOLD effects will be weaker than when using a gradient-echo pulse sequence, leading to a generally lower BOLD contrast. In situations where the susceptibility-induced magnetic field inhomogeneities cause the local T2* to be short, the spin-echo EPI can be considered superior to gradient-echo EPI in detecting the BOLD effect. Also, spin-echo EPI could be used at higher magnetic field strengths where the BOLD effect is larger in order to acquire information on more localized regions of activation.

3. BOLD sensitivity

The gradient-echo EPI pulse sequence offers a high sensitivity to the BOLD effect. The microscopic T2* variations arising from the BOLD effect can, however, be obscured by the effects of macroscopic differences in susceptibility between air, bone and tissue (51,52). Thus, the ability to detect neuronal activation, i.e., the BOLD sensitivity, varies spatially across the brain, as has been observed in emerging clinical applications of fMRI. For example, regions involved in memory functions are particularly prone to susceptibility effects (53-56).

3.1 Calculating the BOLD sensitivity

The BOLD sensitivity (BS) has been defined by Deichmann et al. (57) and by Lipschutz et al. (58) as:

$$BS = TE \cdot I \tag{1}$$

where

$$I \propto \rho \cdot \exp(-TE/T2^*) \tag{2}$$

In Eq. (2), ρ is the local spin density. In Fig. 3.1 the dependence of the BOLD sensitivity on the effective echo time (TE) is shown for several values of T2* calculated with the help of Eqs. (1) and (2). In Fig. 3.1 it can be seen that the BOLD sensitivity is maximal for TE = T2*, as was shown by Gati et al. (59). The effects of macroscopic magnetic field gradients on BOLD sensitivity have been described previously (57,60-62) and are summarized below.

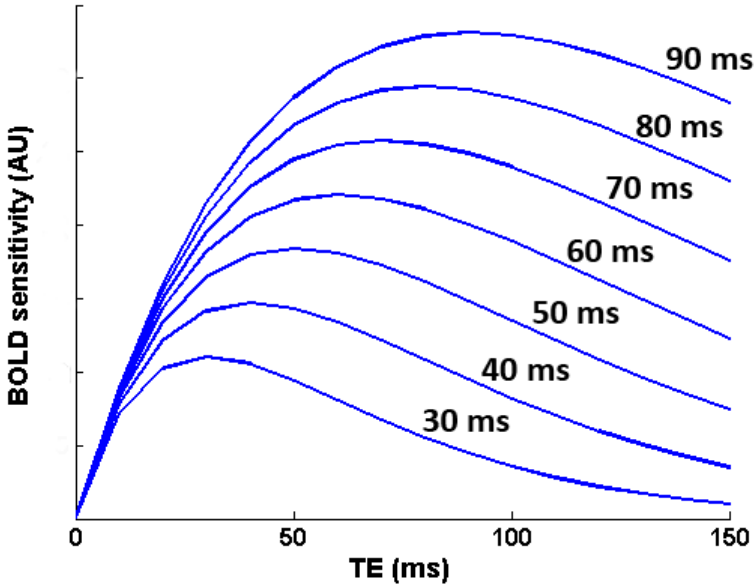

Figure 3.1. Dependence of the BOLD sensitivity on TE for values of T2 between 30 and 90 ms.*

Susceptibility-induced, in-plane magnetic field gradients add to the imaging gradients and therefore distort the *k*-space trajectory. The shift in *k*-space echo location can be defined as $\mathbf{d} = (d_r, d_p, d_s)$ for *k*-space shifts in the readout, phase-encoding, and slice directions, respectively, where **d** is given by:

$$\mathrm{d} = \frac{\gamma}{2\pi} \cdot \mathrm{TE} \cdot \nabla B \tag{3}$$

and B is the macroscopically inhomogeneous magnetic field. For a gradient in the readout direction, the echo will be shifted in the k_r direction, resulting in a sheared *k*-space trajectory (Fig. 3.2 A). In the phase-encoding direction, the result is a stretched or compressed *k*-space trajectory, which can be interpreted as an apparent change in spin density (Fig. 3.2 B). This will affect TE in relation to the nominal echo time as defined in the pulse sequence (TC). The relationship between TE and TC is:

$$\mathrm{TE} = \mathrm{TC} + \frac{d_p}{\Delta k_p} \cdot \Delta t \tag{4}$$

where $\Delta k_p = 1/FOV_p$ and Δt is the inter-echo spacing in the EPI readout. FOV_p is the field of view in the phase-encoding direction. Eqs. (3) and (4) can be combined to calculate TE:

$$\mathrm{TE} = \mathrm{TC} \Big/ \left(1 - \frac{\gamma}{2\pi} \cdot \frac{\partial B}{\partial \mathrm{p}} \cdot \frac{\Delta t}{\Delta k_\mathrm{p}}\right) \tag{5}$$

A predicted image intensity (pII) can then be expressed as:

$$\mathrm{pII} = f_\mathrm{r}(d_\mathrm{r}) \cdot f_\mathrm{p}(d_\mathrm{p}) \cdot f_\mathrm{s}(d_\mathrm{s}) \tag{6}$$

where the three factors $f_\mathrm{r}(d_\mathrm{r})$, $f_\mathrm{p}(d_\mathrm{p})$ and $f_\mathrm{s}(d_\mathrm{s})$ reflect the influence of the magnetic field gradients in the readout, phase-encoding and slice directions, respectively, on the signal. For the readout direction, $f_\mathrm{r}(d_\mathrm{r})$ is given by:

$$f_\mathrm{r}(d_\mathrm{r}) = \begin{cases} 1 \text{ if } |d_\mathrm{r}| < n_\mathrm{r} \cdot \Delta k_\mathrm{r}/2 \\ 0 \text{ otherwise} \end{cases} \tag{7}$$

where n_r is the k-space matrix size in the readout direction. The image intensity is unaffected as long as the central echo obtained at TE is not shifted outside the acquisition window. The effect on the signal due to magnetic field gradients in the phase-encoding direction is given by:

$$f_\mathrm{p}(d_\mathrm{p}) = \begin{cases} \frac{\mathrm{TE}}{\mathrm{TC}} \cdot \exp\left(-(\mathrm{TE}-\mathrm{TC})/\mathrm{T2}^*\right) \text{ if } t_\mathrm{start} < \mathrm{TE} < t_\mathrm{end} \\ 0 \text{ otherwise} \end{cases} \tag{8}$$

where t_start and t_end are the points in time after excitation at which acquisition starts and ends, respectively.

Finally, the effects of a susceptibility-induced gradient in the slice selection direction causes through-plane spin dephasing (Fig. 3.2 C). The factor $f_\mathrm{s}(d_\mathrm{s})$ can be expressed as the Fourier transform of the slice profile, which for a gaussian profile yields:

$$f_\mathrm{s}(d_\mathrm{s}) = \exp\left(-\left(d_\mathrm{s} \cdot \pi \cdot \Delta z / \left(2 \cdot \sqrt{\ln 2}\right)\right)^2\right) \tag{9}$$

where Δz is the slice thickness. Paper I presents the validation of the above expressions for the effects of susceptibility-induced magnetic field gradients. EPI images of a phantom were obtained together with corresponding field maps

acquired in order to calculate the magnetic field gradients. A range of known gradients was obtained by deliberately misadjusting the shim coils, and the predicted image intensity was compared with the EPI image signal intensity. It was found that better correspondence was obtained between the experimental and the theoretical image intensities when an expression for a rectangular slice profile was used instead of the gaussian slice profile above (Eq.(9)). Assuming a rectangular slice profile, the expression for $f_s(d_s)$, becomes:

$$f_s(d_s) = \mathrm{sinc}(d_s \cdot \Delta z) \tag{10}$$

The predicted BOLD sensitivity (pBS) can then be derived from pII as:

$$\mathrm{pBS} = \mathrm{pII} \cdot \frac{\mathrm{TE}}{\mathrm{TC}} \tag{11}$$

where the second factor reflects the change in TE.

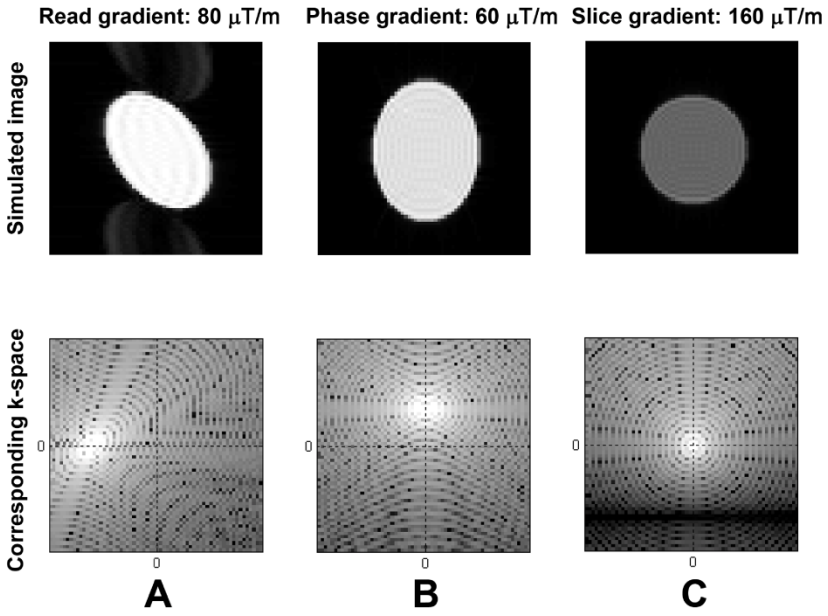

Figure 3.2. Simulated images of a cylindrical object (top row) and the corresponding k-space (bottom row) showing the effects of uniform linear gradients in: (A) the readout direction (80 μT/m), (B) the phase-encoding direction (60 μT/m) and (C) the slice selection direction (160 μT/m).

The field map used to calculate the magnetic field gradients in the study described in Paper I was acquired using a double-echo gradient-echo pulse sequence (45). The phase evolution resulting from magnetic field inhomogeneities can be scaled to represent the actual magnetic field distribution by extracting the phase difference between the first and second echo.

Fig. 3.2 (upper row) shows that the effects on the *k*-space trajectory caused by in-plane, susceptibility-induced magnetic field gradients also manifest themselves as a distortion of the image. This effect can be corrected by the use of field maps, i.e., the local magnetic field can be scaled to represent the actual amount of spatial shift of the signal, which can then be reversed, resulting in a distortion-corrected image.

Signal loss due to susceptibility effects has been studied by Ojemann et al. (63) in gradient-echo EPI images, and also by Lipschutz et al. (58), who proposed a method of characterizing signal changes using only the functional EPI data. As can be seen from the definition of BOLD sensitivity (Eq.(5)), the effects of variation in local TE must, however, also be considered. Maps of BOLD sensitivity, taking the echo time effects into account using a double-echo gradient-echo pulse sequence, have been utilized in studies by Cusak et al. (60) and in the present work (Paper I). Maps of BOLD sensitivity can also be obtained by using complex *k*-space data (57,61,62,64).

Reliable assessment of BOLD sensitivity can indeed be obtained by the use of field maps. In the study described in Paper I, the assumptions underlying the theory were validated, and it was found that the correct choice of slice profile is important. A slight offset in the results obtained for the predicted image intensity was also observed, probably due to a pulsed gradient, possibly an imperfectly refocused slice selection gradient. Thus, the effects of slice profile and additional gradients must be assessed in order to obtain accurate maps of BOLD sensitivity or predicted image intensity. A field map can be obtained with an additional scan time of approximately 30 s, which is feasible in the clinical setting.

However, the assumption that a single field map is valid for a full fMRI experiment must also be verified. Subject motion and positioning will lead to changes in the gradients, predominantly in the slice and phase-encoding directions, depending on their relation to the main magnetic field. The dependence on orientation has been investigated by Deichmann et al. (61), and an analytical model describing these effects has been proposed by Andersson et al. (65). Paper I describes the effects of subject motion and positioning. A finger-tapping paradigm was performed by one subject while repeated field maps were acquired. The maximum translation and

rotation during the performance of this task were 1.3 mm and 1.6°, respectively. These values are within the normal range, although somewhat larger than those found in other studies of patient motion. Seto et al. (66) found translational motion in a group of stroke patients to be approximately 2 mm, while the translational motion was smaller for a control group of healthy volunteers. In a study by Hill et al. (67), foam padding and head restraining bands were used to limit motion. The median values of translational motion and rotation in that study were below1 mm and at most 0.5° for both epilepsy patients and volunteers. Thus, the use of a single field map is feasible when assessing the BOLD sensitivity for a complete fMRI experiment.

The study by Deichmann et al. (61) indicated that subject positioning can have a considerable impact on the magnetic field distribution across the brain, and hence influence the BOLD sensitivity. This was confirmed in the study presented in Paper I, where the BOLD sensitivity in the hippocampus was found to be significantly affected by the choice of subject positioning in terms of head pitch relative to the main magnetic field. The effect of head pitch could thus be utilized to minimize the effects of susceptibility-induced gradients in studies focused on cognitive functions, including memory and awareness, localized in the orbitofrontal cortex and in the medial temporal lobe.

The value of the BOLD sensitivity is by definition 1 when no susceptibility-induced gradients are present. Interestingly, BOLD sensitivity values larger than unity were observed in the hippocampus region (Paper I). This could arise from a magnetic field gradient in the phase-encoding direction, as long as the acquired central echo still lies within the sampled *k*-space. Thus, the fact that the BOLD sensitivity was found to be larger than unity in most parts of the hippocampus contradicts the results of previous studies explaining the inability to find neuronal activation in these areas of the brain by the presence of susceptibility-induced gradients (55).

Another application of fMRI for presurgical mapping is the determination of language laterality. This is achieved by means of laterality indices, i.e., by determining the relation between active voxels in the right and left parts of the language area. This could be hampered if the BOLD sensitivity varies from right to left in the brain, as was systematically found in a group of 8 volunteers in the present work (Paper I). It was concluded that this effect arose from a large-scale, right-left magnetic field gradient, most probably due to magnetic field

inhomogeneities in the MRI system, but also, in part, to a slight asymmetry in the standard regions of interest used.

The mapping of BOLD sensitivity by means of field maps and the expressions given above are important in providing information about the effects of susceptibility-induced magnetic field gradients on the EPI images. However, maps of BOLD sensitivity or predicted image intensity are not directly related to the final statistical maps. Nevertheless, the existence of false-negative voxels in the statistical maps can result from low or zero BOLD sensitivity, implying that information about BOLD sensitivity is of importance.

3.2 Improving the BOLD sensitivity

Several methods aimed at improving the BOLD sensitivity have been proposed. One approach is to optimize the shimming of the magnet, which can be performed directly on the MRI scanner. The use of an intra-oral diamagnetic passive shim device has also been proposed (60,68). The use of tailored RF pulses is another approach, in which an RF pulse with a quadratic phase distribution along the slice selection direction effectively cancels out phase dispersion effects from local susceptibility-induced gradients (69). However, this method introduces dephasing of regions not affected by susceptibility effects. A 3D version of this concept, minimizing this drawback, was later suggested by Stenger et al. (70).

Another commonly used method is the so-called *z*-shimming technique (71-74). This technique utilizes preparation gradient pulses in the slice selection direction when constructing a series of images. These images can then be combined in order to recover signal loss. Glover et al. proposed a 3D version of *z*-shimming that can also be used for compensation of in-plane susceptibility gradients.

BOLD sensitivity is also affected by the voxel size of the EPI images due to partial volume effects, and the spatial resolution can thus be increased to reduce the effects of susceptibility-induced gradients (75,76). However, reducing the voxel size leads to a lower signal-to-noise ratio (SNR), potentially reduced spatial coverage and lower temporal resolution.

4. Data analysis strategies for fMRI

The methods of analysing fMRI data can be broadly classified into two approaches. Historically, the most commonly used method of analysis relies on the specification of a model for the expected time course of an activated voxel. The most flexible framework for modelling activation-related time courses is the so-called general linear model (GLM). The second approach avoids modelling which, to some extent, introduces uncertainties regarding the expected temporal characteristics of an activated area. Methods related to the latter approach are classified as data-driven methods, and are characterized by the fact that no assumptions are made regarding the expected temporal characteristics of the fMRI data. These two kinds of analysis will be described below and discussed with respect to their inherent strengths and weaknesses.

4.1 Preprocessing

Several preprocessing steps are usually performed before any statistical analysis can be made of acquired fMRI data. The purpose of the preprocessing is to remove various kinds of artefacts in the data. Also, preprocessing conditions the data in order to increase the sensitivity of the subsequent statistical analysis.

4.1.1 Slice timing correction

The first preprocessing step is often the correction of slice timing. This step compensates for the fact that the individual slices of a volume are normally acquired at time points equally spaced over the whole TR, meaning that the time courses of the first and last slice in the volume can be offset by the duration of TR. Therefore, the data are adjusted so that it appears as though all the slices were acquired at the same time, which allows the whole data set to be modelled using a single reference function in the subsequent analysis step.

4.1.2 Correction for subject motion

Subject motion can be a major source of error in fMRI data. If the patient moves during the examination, the recorded time series for a particular voxel will not

correspond to the same location in the brain. Assuming the volumes are rigid bodies and that subject motion introduces no systematic change in global image intensity, subject motion can be represented by 3 rotations and 3 translations. In order to align an image volume to a reference volume, for example, the first volume (77) or a calculated mean volume (78), the required translations and rotations can be computed by minimization of the squared differences over all voxels. An additional effect of subject motion is the so-called spin-history effect. This effect arises from the fact that the position-dependent image intensity at a certain point in time will also be dependent on the position at a previous point in time. The effects of spin history can be modelled and removed from the time course of each voxel utilizing the motion parameters described above (77).

4.1.3 Spatial filtering

At this stage, spatial smoothing of each volume is often employed, normally by convolution of each volume by a 3D gaussian kernel, which increases the SNR. As spatial smoothing introduces weighted local averaging to the images, the random noise will cancel out, while the underlying signal will be retained. However, the width of the smoothing kernel should match the expected size of the activated region. If, for example, a filter width greater than the width of the activated region is used, the contribution from non-activated areas will be large in the averaging process, reducing the signal from the activated area. An additional reason for performing spatial smoothing of the data is that later statistical processing requires the images to be spatially smooth (79).

4.1.4 Temporal filtering

The purpose of temporal filtering is to remove unwanted components from the voxel time series. Examples of such confounding signals in fMRI data are slowly varying, scanner-related drift and physiological noise arising from the cardiac cycle or breathing. Slowly varying signal fluctuations can be removed by high-pass filtering, and this is important even if the noise is not correlated to the experimental paradigm. Since such noise will result in poorer fitting of the model to the data, the residuals will be higher, reducing the statistical significance. However, it is necessary to determine the appropriate setting of the cut-off frequency in order not to reduce the signal of interest in a block-designed experiment.

Low-pass filtering can also be performed. This can be implemented as the spatial smoothing described above, i.e., a convolution of a time series with a gaussian

kernel, smoothing the time series. As for high-pass filtering, it is important to select the appropriate cut-off frequency in order to remove noise without attenuating the underlying signal of interest. For example, when an event-related paradigm is used, too much smoothing could suppress signals arising from a single event, thus reducing the power of the subsequent statistical analysis.

4.1.5 Spatial registration and normalization

Additional preprocessing steps include coregistration of a structural image in order to facilitate the final overlay of the activation maps resulting from the statistical analysis, onto this high-resolution image. This improves the interpretation of the statistical results, as anatomical structures are easier to observe in a high-resolution image than in the EPI images, which have inherently lower resolution. The coregistration of images with different contrasts, however, requires a different strategy from that described above concerning realignment of images of the same type, for example, coregistration of a T1-weighted high-resolution image with a low-resolution T2*-weighted image. This situation requires another measure of similarity between the two types of image. Several such similarity measures have been proposed, e.g., mutual information (80,81) and the correlation ratio (82). The transformations that maximize the similarity between two images can then be found using various optimization algorithms. Also, the coregistration of images with different contrasts or resolutions differs from the rigid body translations described above in the inclusion of linear local scaling and shearing, as well as translation and rotation (so-called affine transformations). Coregistration can also be extended to include non-linear transformations, although additional constraints must be imposed in order to preserve the topology of the images.

Non-linear spatial registration algorithms can be used when performing a study in which inference is drawn from a whole group of subjects (83). The volumes can be transformed into a common standard space, a step often referred to as spatial normalization. This is performed by transformation of the volumes in order to obtain a good match between a template image, normally derived from the averaging of multiple individual brain images, and the brain volume of the individual subject. The two most widely used standard spaces are the Montreal Neurological Institute space (84) and the roughly corresponding Talairach space (85). When fMRI is used in a clinical setting, the normalization step is normally omitted, but can be used, for example, when assessing language lateralization, facilitating the use of standardized regions of interest defined in standard space.

4.2 The general linear model

Following the preprocessing steps, statistical analysis is performed in order to determine which voxels are activated by the stimulus. The GLM, currently the most popular method, provides a univariate analysis, i.e., the time course of each voxel is analysed independently (86,87). The GLM is based on the specification of a model, i.e., a general signal time course which is expected to be seen in voxels corresponding to locations in the brain that have become active in response to the applied stimulus. This model is then fitted to the observed data and statistical inference can be drawn. The measured data are expressed as a linear combination of one or several *explanatory* variable(s) plus some residual error, reflecting the amount of variation in the observed data that is not accounted for by the explanatory variables. Applied to fMRI data, the GLM for a *response* variable x_{ij} (the measured signal value) at voxel $j = 1, \ldots, J$ can be expressed as:

$$x_{\mathrm{ij}} = g_{i1}\beta_{1j} + g_{i2}\beta_{2j} + \cdots g_{iK}\beta_{Kj} + e_{ij} \tag{12}$$

where $i = 1, \ldots, I$ indexes the scans. The coefficients g_{ik} are the explanatory variables that describe, for example, the experimental design in terms of onsets of stimuli. Other measures that might reflect the conditions under which the measured data were acquired, such as motion-related parameters, can also be included. The relative contribution of each explanatory variable is represented by β_{kj} (K unknown parameters for each voxel j). The residual errors, e_{ij}, are assumed to be independent and identically normally distributed $N(0, \sigma_j^2)$. The GLM can be reformulated using matrix notation to give:

$$\mathrm{X} = \mathrm{G}\boldsymbol{\beta} + \mathrm{e} \tag{13}$$

where X is the measured data matrix with one column for each voxel j and one row for each scan, i, corresponding to entries x_{ij}. The matrix G is called the design matrix and is composed of the explanatory variables g_{ik}. The unknown parameters are contained in the column matrix $\boldsymbol{\beta}$, and the residual errors in e. The GLM, as stated here, does not contain any constant terms. This is normally remedied by adding a column of ones to the design matrix G (Fig. 4.1), or by mean correcting the data. The model is then fitted to data by a least-squares estimation of the parameters, $\hat{\boldsymbol{\beta}}$:

$$\hat{\beta} = \left(G^T G\right)^{-1} G^T X \tag{14}$$

In order to convert the parameter estimates $\hat{\beta}$ into a useful statistic, they are compared with the uncertainty in their estimation, which produces a t-statistic such as:

$$t = \frac{c^T \hat{\beta}}{\sigma \sqrt{c^T \left(G^T G\right)^{-1} c}} \tag{15}$$

where the numerator expresses the size of the effect in terms of estimated $\hat{\beta}$, and the denominator is the standard error of the estimates. The factor σ is the standard deviation of the residuals and c denotes the so-called contrast vector, which defines the combination of explanatory parameters that is to be tested. This makes it possible to describe how each voxel is related to each explanatory variable. For example, a simple contrast vector could be created, comparing only the activation resulting from a finger-tapping task to the rest condition in a blocked paradigm. Using the contrast vector, an experiment described by multiple explanatory variables (e.g., denoting the existence of several experimental conditions or reflecting motion parameters) could then be analysed using several different contrasts in order to investigate how combinations of different conditions affect activation.

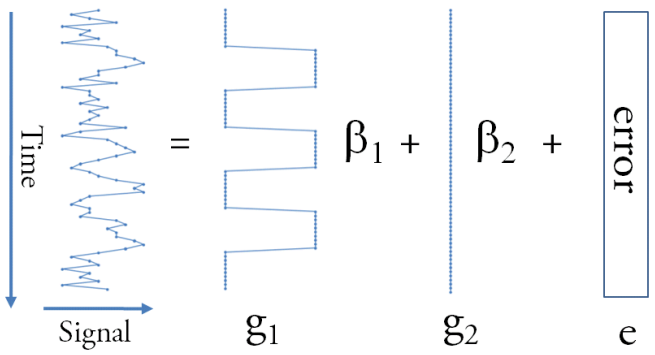

Figure 4.1. Graphical illustration of GLM applied to signal from a single voxel. A blocked paradigm is represented by the regressor g_1, and the constant term correspondingly represented in g_2.

Most commonly in fMRI, the model for the different conditions is specified by defining the columns of the design matrix G as integers, in order to denote whether a stimulus or task is present or not at a certain point in time

(corresponding to ones or zeros in the design matrix). Since this corresponds to a naïve boxcar model of the actual time course of a voxel being activated in response to the condition, convolution with a function reflecting the characteristics of the haemodynamic response function of a brief stimulus (cf. Section 2.1.2) makes the model more physiologically plausible. The haemodynamic response function has been modelled as a single gamma function (88), and was later extended to a combination of two gamma functions, making it possible to capture the post-stimulus undershoot (89).

The t-test in Eq. 15 results in a statistic map from which inference can be drawn. Which parts of the brain were active is determined by thresholding the map at a given level of significance (p). Those voxels exceeding the threshold can be colour-coded and overlaid on an image containing anatomical information (Fig. 4.2).

However, a problem with this approach is that many voxels have been tested for statistical significance. This multiple comparison problem introduces a large number of voxels falsely determined as activated. If, for example, 50000 voxels are tested at a significance level of $p<0.01$, then it would be expected that 500 voxels were falsely classified as activated. The use of gaussian random field theory (90) or the false discovery rate (91) method are, however, techniques that can be used to correct for the number of false positive voxels.

The flexibility of the general linear model, in terms of modelling different paradigms and constructing contrasts when making statistical inferences, can also be used to increase confidence in detecting the BOLD signal in cases where subject compliance can be expected to be low. This can be a problem in the clinical use of fMRI, for example, when a patient cannot fully comply with the instructions given with regard to the performance of a specific task. In Paper II, the impact of reduced task compliance was reported. Modelling each block in a block-designed paradigm as a separate column in the design matrix accounts for possible lower response due to non-compliance in one or several blocks. However, increasing the number of columns in the design matrix reduces the degrees of freedom, which leads to lower statistical power. Thus, the use of a flexible model was compared with the use of only one column as a model for the full fMRI experiment. This analysis was performed using simulated and experimental data, as well as the reanalysis of 14 fMRI data sets from patients who had previously been examined using a single explanatory variable. Simulated and experimental data were constructed to represent decreasing levels of subject compliance.

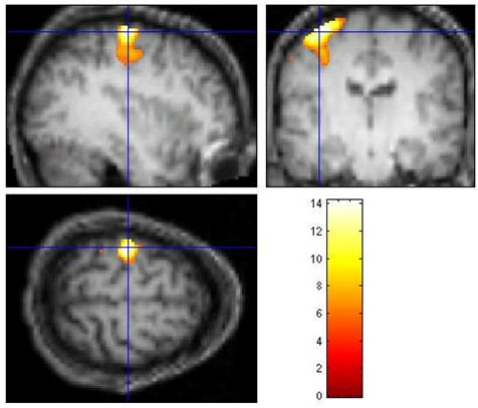

Figure 4.2. Resulting thresholded map of t-values overlaid on the mean EPI volume from the whole data set. The statistically significant activation (shown in colour) corresponds to the primary motor cortex in response to a finger-tapping task.

Both experimental and simulated data confirmed that even at 80% compliance (corresponding to a subject not performing the required task during one of five blocks), a flexible model outperforms standard statistical analysis. Furthermore, the retrospective analysis of clinical fMRI examinations revealed that using the flexible model yielded a gain in model performance with little or no penalty with regard to sensitivity. Hence, in cases where patient non-compliance can be expected, the use of a flexible model should be considered as this increases the probability of a successful fMRI examination.

4.3 Data-driven analysis methods

Although the GLM has proven to be a very robust method for the analysis of fMRI data, the obvious drawback of the method is the need to specify a model. As stated above, this renders the GLM less sensitive in cases where the model is misspecified. Any method relying on a model can only extract information about how well the observed data are explained by the model. This implies that it may be advantageous to use a different kind of method allowing exploratory analysis of fMRI data. These exploratory methods do not rely on any model, but impose assumptions with varying degrees of stringency on the data distributions. In this section, two established methods of model-free analysis of fMRI data are presented, together with an alternative method.

4.3.1 Principal component analysis

A general approach when performing model-free analysis is to reduce the inherent dimensionality of the data to a lower dimensionality and, in doing that, capture the characteristics of the data. The basic idea of principal component analysis (PCA) is to characterize the data in terms of covariance. The data can be described by a 2D matrix, X, with v columns representing the individual voxels of an EPI volume, and n rows representing the scans. The covariance between, for example, the individual data volumes, can now be constructed yielding a covariance matrix of size $n \times n$. By calculating the n eigenvectors of the covariance matrix, so-called principal components are extracted. Forming a matrix, W, of eigenvectors as rows yields the following representation of the data:

$$Y = WX \tag{16}$$

where the resulting data after PCA are represented by the matrix Y, obtained by transformation of the original data, X, by multiplication with the eigenvector matrix, W. This represents a rotation of the coordinate system. The first principal component goes through the maximum variation in the data and explains most of the variance in the data. Since all principal components are orthogonal, i.e. uncorrelated, they account for decreasing amounts of variance in the data. The relative amount of variation explained by the different principal components (eigenvectors) is governed by the eigenvalues, i.e., the eigenvalue of the first eigenvector is largest, explaining most of the variance. Hence, the rows of W correspond to eigenvectors with correspondingly decreasing eigenvalues. This can be utilized to reduce the dimensionality since less important principal components

(i.e. those with small corresponding eigenvalues) can be omitted from W since they make a very small contribution to the explained variance. Hence, a data set can finally be represented as Y in a more compact sense, without losing its inherent characteristics. For fMRI data, PCA can be seen as a reduction in, for example, the time dimension. In a typical fMRI experiment, a total of approximately 100 time points are used (i.e., 100 volumes of EPI data are acquired during the experiment). This number can be regarded as the original dimensionality of the data. By performing PCA and selecting those principal components that account for a predetermined amount of variance (e.g., 90%), a significant reduction along that direction can be obtained, reducing the data set along the time dimension from 100 to, for example, 20-40. Thus, the dimensionality-reduced data set can now be represented as 20-40 spatial components, where each component is uncorrelated with respect to the rest of the data set.

The components resulting from dimensionality reduction of fMRI data correspond to spatial maps with an associated characteristic time course. Hence, some components reflect task-related activation, while others reflect artefactual activation, such as patient motion or respiratory-induced activation.

4.3.2 Independent component analysis

Although PCA can be used to compress fMRI data, and to reflect the essential characteristics, a stronger criterion can be applied to the relationship between individual voxel time courses. This can be achieved by independent component analysis (ICA), where a rotation matrix is introduced that makes the components as statistically *independent* as possible, in contrast to the components' being *uncorrelated* using PCA (92,93). The estimates can thus be improved when decomposing fMRI data into separate components. Using PCA, the characteristics of the matrix W lead to the final component maps in the matrix Y being uncorrelated, whereas using ICA, the matrix W is selected so that the data in Y are maximally statistically independent.

When performing ICA, the data are assumed to consist of linearly mixed components. When trying to find the original components, assumed to be statistically independent, ICA relies on the fact that linearly mixed signals are more gaussian than the original sources, which is a reformulation of the central limit theorem. When determining W, the so-called mixing matrix, ICA algorithms therefore minimize the gaussianity of the mixed signals, which can be parameterized using metrics such as kurtosis or negentropy. This can be described as rotating the coordinate axes individually, in contrast to PCA where the whole

coordinate system is rotated, thus potentially yielding non-orthogonal axes. It should be noted that ICA is normally preceded by a reduction in dimensionality utilizing PCA.

The use of ICA for the analysis of fMRI data was first suggested by McKeown et al. (94), in a study showing that ICA was capable of isolating spatial patterns of activation with characteristic time courses, such as task-related or transiently task-related components. Artefactual components relating to abrupt or slow head movement were also identified. Furthermore, it was shown that the characteristic time courses obtained from a task-related component using ICA were significantly better correlated to the imposed task reference function than those obtained using PCA. Several ICA algorithms have been proposed, e.g. FastICA (95,96) and Infomax (97).

4.3.3 Non-linear dimensionality reduction

Although PCA has been shown to provide robust results when used for dimensionality reduction, only linear decomposition of the data is possible, which may not be sufficient to capture, for example, non-linear subject motion (98). Others have challenged the assumption that sources are linearly mixed, and have thus suggested the use of non-linear approaches (99,100). More recent studies have suggested the use of Laplacian embedding (101) and the diffusion map algorithm (102).

An example of an artificial data set with non-linear properties is shown in Fig. 4.3, illustrating how PCA fails to capture the underlying characteristics, whereas an algorithm that is designed to perform non-linear dimensionality reduction can extract the true characteristics. Fig. 4.3 shows the so-called Swiss-roll data set with an intrinsic dimensionality of 2, embedded in a 3D representation (left). PCA cannot be expected to unfold this data set (middle), whereas this can be accomplished by a non-linear dimensionality reduction algorithm (right). The non-linear algorithm used in this example is the locally linear embedding (LLE) algorithm, originally proposed by Roweis and Saul (103), and used as a tool for dimensionality reduction of fMRI data in the study described in Paper III.

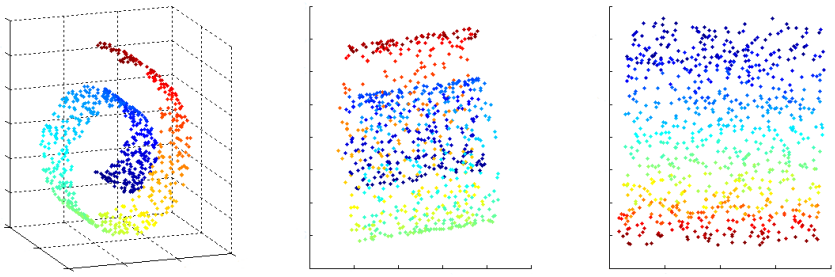

Figure 4.3. The Swiss-roll data set (left), which is a 2D data set embedded in 3D. PCA fails to unfold these data (middle), whereas LLE can map the data into their true 2 dimensions (right).

Briefly, non-linear dimensionality reduction techniques try to preserve some property of the original data in the process of reducing it to a low-dimensional representation. Examples of such properties are global or local distances. Algorithms that preserve global properties are, for example, the Isomap algorithm (104) and the multi-dimensional scaling (MDS) algorithm (105). These algorithms preserve pairwise distances between the data points. The MDS algorithm uses Euclidean distances, which may lead to erroneous short-cuts in a data set with characteristics such as the Swiss-roll example. Isomap, on the other hand, preserves geodesic distances, which avoids short-cutting. Algorithms that try to preserve local distances include LLE and the Laplacian eigenmap algorithm (106).

The purpose of LLE is to find a compact representation of a data set, i.e., one corresponding to the representation of the data in terms of principal components in PCA. However, LLE does not summarize the data in terms of how much variance is explained by choosing a number of eigenvectors from a covariance matrix. Instead, LLE does this by finding an embedding of lower dimensionality that preserves local relationships. Thus, the low-dimensional embedding will have similar characteristics to the original high-dimensional data representation in terms of the distance between points. This means that nearby points in the high-dimensional input data will remain nearby in the dimensionality-reduced representation. This is achieved by representing each point as a linear patch created from its nearest neighbours. For fMRI data, this can be thought of as creating patches of voxels with similar time courses. The patches can then be described as linear coefficients that reconstruct each point from their neighbours. By minimizing the sum of the squared distances between all the data points and their reconstructions, an optimal reconstruction of the data can be obtained from:

$$\varepsilon(W) = \sum_{i=1}^{N} \left\| \vec{X}_i - \sum_{j=1}^{N} W_{ij} \vec{X}_j \right\|^2 \quad (17)$$

where $\varepsilon(W)$ is the cost function to be minimized. The coefficients W_{ij} contain the contribution of the *j*th data point to the reconstruction of the *i*th point. The time course of each voxel in the fMRI data set is contained in the vector $\vec{X}$. The low-dimensional representation of the data can now be obtained by constraining the coefficients W_{ij}, which retain the geometrical properties of the data in the low-dimensional mapping. The final step is to minimize the reconstruction error when transforming the data into its low-dimensional representation:

$$\Phi(Y) = \sum_{i=1}^{N} \left\| \vec{Y}_i - \sum_{j=1}^{N} W_{ij} \vec{Y}_j \right\|^2 \quad (18)$$

The cost function in Eq. (18) is similar to Eq. (17), and minimizes the reconstruction error. However, in this case, the coefficients in W_{ij} are fixed, and the low-dimensional output vectors $\vec{Y}$ are reconstructed.

The final step in LLE is an eigenvalue problem, and by solving for a suitable number of eigenvalues, decomposition of the data is obtained in the same way as for PCA.

LLE was applied to simulated and experimental fMRI data and the proposed concept was evaluated and optimized (Paper III). The algorithm has one free parameter, i.e., the number of neighbouring points used when constructing the locally linear patches. It was found that the choice of neighbourhood size was not critical, and that task-related components as well as motion-related components could be reliably obtained. The results of the algorithm compared well with those obtained using PCA. Using an example data set with non-linear properties to simulate the physiologically plausible assumption of a delayed haemodynamic response (34,35), it was shown that LLE could separate a group of active voxels from non-active ones, whereas neither PCA nor non-linear PCA could achieve this. Furthermore, LLE was applied to a resting-state data set and several networks were identified by the algorithm. Hence, it is reasonable to conclude that LLE can be used as a preprocessing step for ICA, with potential advantages when analysing fMRI data sets pertaining to patients with a delayed haemodynamic response.

5. Resting-state fMRI

The resting brain, represents only 2% of the total body mass and consumes 20% of the available energy, although the task-related increase in neuronal metabolism is less than 5% (16,107). Thus, a significant degree of neuronal activation cannot be accounted for by task-related fMRI experiments. Spontaneous neuronal activation in subjects at rest was first observed using BOLD fMRI in a study by Biswal et al. (15), where time courses of low frequency (<0.1 Hz) were found to exhibit significant correlation within the sensorimotor cortex. Similar results have been reported in several subsequent studies (108-112). The frequency distribution of resting-state fMRI signals has been further investigated by Cordes et al. (113), who showed that signals from functionally connected cortical networks found using resting-state measurements were predominantly of low frequency.

5.1 Analysis of resting-state data

The purpose of analysing resting-state data is to find functional connectivity between brain voxels. This connectivity corresponds to areas in the brain with coherent signal variations over the course of the experiment. The simplest technique for the identification of functionally connected networks is to extract the mean time course for a region of interest, a so-called seed region. This time course is used as a reference function, and the correlation with all other brain voxels can be analysed. In order to find low-frequency time courses, the data are temporally filtered using a low-pass filter with a cut-off frequency of approximately 0.1 Hz before correlation analysis (15,113). Although simple, this technique has the disadvantages of relying on a well defined region of interest, and of only being able to investigate a single network.

One concern associated with resting-state fMRI measurements is that the signals can be contaminated by non-neuronal physiological fluctuations arising from, for example, the cardiac cycle or respiration. Several strategies have, however, been employed to address the possible influence of such non-neuronal noise on the resting-state signal. Physiological parameters can be measured (e.g., by using a pulse-oximeter to monitor the cardiac cycle, or a pneumatic belt to monitor respiration) and subsequently modelled as covariates of no interest using the GLM (cf. Section 4.2) (114). Alternatively, physiological noise parameters can be

obtained from areas where artefactual signals can be expected to be significantly larger than neuronal activity, for example, in cerebrospinal fluid or white matter (115,116). The global signal, being common to all voxels, can also be used as a covariate of no interest (115,117,118).

By using a data-driven algorithm instead, such as ICA or LLE (Paper III), noise sources are isolated into separate components, and specific modelling of these sources can be omitted. Also, a data-driven algorithm does not require the specification of a seed region, and decomposition of the data into multiple-component maps can identify several functionally connected networks. A disadvantage of using ICA is the need for interpretation of the component maps. This has been addressed by De Martino et al. (119), who suggested the use of spatial and temporal parameters characterizing each component, thereby facilitating the classification of each component into, for example, BOLD-related or artefactual components.

5.2 Resting-state networks

Following the initial observations that the sensorimotor system shows coherent temporal characteristics, several networks have been shown to exhibit coherent activity at rest, including the visual system, the auditory system, the language system, the dorsal attention system, the frontoparietal system and the default mode network. The default mode network is also active during the execution of a task, but is attenuated relative to resting conditions. The default mode network has been found to be active when subjects are engaged in remembering the past, imaging future events and during self-referential thoughts (120).

Although spontaneous activation was originally observed in adult subjects during awake rest, these networks have also been observed under other conditions. Spontaneous activation has been shown to persist during periods of extended rest and sleep (121-125), and also under the influence of anaesthesia (126,127). Furthermore, resting-state activation has been used to map several networks in the infant brain (128-130).

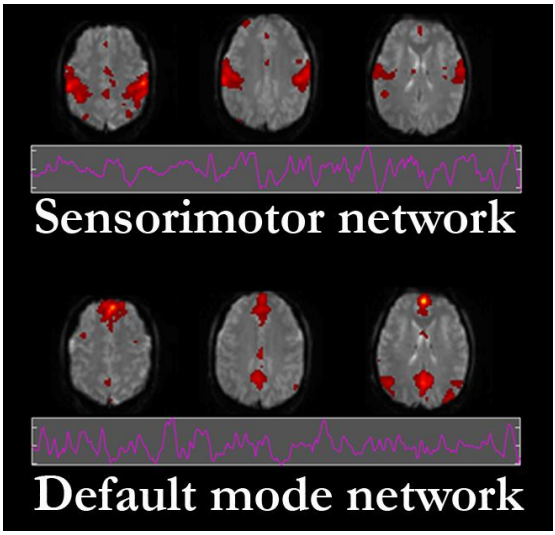

Figure 5.1. Example slices showing spatial maps and characteristic time courses for the sensorimotor network (top row) and the default mode network (bottom row) in a single subject. The data were analysed using ICA.

5.3 Clinical applications of resting-state networks

The study of spontaneous activation using fMRI offers the possibility to gain deeper insight into the dynamics of the brain, and its maturation and evolution. Several clinical applications of resting-state fMRI may also be of interest. A number of studies have focused on comparing normal subjects with patients with neurological or psychiatric diseases, to determine whether the appearance of spontaneous activation can be used as a diagnostic or prognostic tool. Disturbances in resting-state networks have been demonstrated in patients suffering from, e.g., Alzheimer's disease (131-134), multiple sclerosis (135,136), depression (137-139), schizophrenia (140-143), epilepsy (144) and attention deficit hyperactivity disorder (145-147). It has been suggested that information could be obtained about the severity of disease and recovery from disease-related functional deficits, and applied clinically through the study of changes in these networks.

Another clinical application could be the use of resting-state fMRI as a presurgical mapping method. Presurgical mapping has been implemented by using traditional task-based fMRI, in order to map functional areas at risk, thereby providing the neurosurgeon with information on the risk of functional deficits following brain surgery (17-23). In certain cases, it can be difficult to perform task-based fMRI, for

example, in non-compliant patient groups such as children, or in patients with severe disease-related impairment. The use of resting-state fMRI in such patient groups may thus be a feasible complement, provided that networks corresponding to areas in the vicinity of, for example, a tumour can be reliably detected.

5.4 Reliability of resting-state networks

If resting-state fMRI is to be considered feasible in a clinical setting, the reliability of the detected networks must be assessed, and several studies have addressed this issue. Significant overlap of activated areas for both hand and tongue activation was found in a group of surgical candidates by Chen et al. using the seed-based method (148). The same approach was used by Shimony et al. (149), who demonstrated the feasibility of resting-state measurements for presurgical mapping in tumour patients. A drawback of using the seed-based method in a clinical setting is that the anatomical information required to define an appropriate seed region might not be available. Anatomical landmarks of different functional areas are not always present, and may be severely distorted, for example, in patients with a tumour. This drawback can, however, be avoided by the use of a model-free method such as ICA.

The studies by Chen et al. and Shimony et al. did not address the repeatability of the registration of the spontaneous networks, an aspect which is crucial in any method being considered as a clinical tool. This was addressed by. Chen et al. (150) who showed that a number of resting-state networks are consistent over time, while good reliability between two sessions was observed by Van Dijk et al. (151) in a study using spatial overlap of activated areas as a reliability measurement.

Paper IV presents a test-retest reliability investigation on group of 10 healthy volunteers, based on a method described by Genovese et al. (152) and Noll et al. (153). This method yields estimates of true-positive and false-positive ratios, which can be assessed for a range of statistical thresholds. These estimates constitute a receiver operating characteristic (ROC) curve, and reliability can be assessed using the area under the ROC curve as a quantitative measure. It was found that resting-state sensorimotor networks assessed using ICA compared well with corresponding areas activated using a bilateral finger-tapping paradigm. In most cases, the area under the ROC curve was smaller for the resting-state measurements than the corresponding area for task-based fMRI. However, the differences were not large, and were not significant on a group level. The results presented in Paper IV,

together with those of other studies investigating the reliability of resting-state measurements, suggest that this method could be used as a supplement to traditional task-based fMRI examinations in a clinical setting.

6. Concluding remarks

In BOLD fMRI, it is of considerable relevance to characterize the local sensitivity to the BOLD effect. The dominating pulse sequence used for BOLD fMRI is the gradient echo EPI, which allows rapid imaging with good spatial coverage. The EPI pulse sequence is, however, inherently sensitive to susceptibility-induced magnetic field gradients, which potentially impairs the BOLD sensitivity in certain regions. In Paper I, the method of utilizing field maps was verified and an expression for an alternative slice profile was proposed. Furthermore, the verified expressions were used to investigate how the characteristics of a typical clinical MRI system influenced the BOLD sensitivity in a group of healthy volunteers. It was also established that a field map is valid for an entire fMRI experiment under normal subject motion, i.e. a reliable BOLD sensitivity map can be derived from a single field map.

Patient compliance is a limiting factor in the clinical use of fMRI, and several methods have been introduced to make fMRI clinically useful even if patient compliance is restricted. The modeling of each block of activation in a clinical paradigm as a single regressor is an easily implemented approach that increases the sensitivity of fMRI data analysis in subjects unable to fully comply with a normal clinical paradigm (Paper II). In simulated, experimental and retrospectively analyzed clinical fMRI examinations, the use of a flexible model yielded a gain in model performance. Hence, a flexible model is a feasible approach that could improve reliability of clinical fMRI.

Data-driven methods are not in widespread use for analysis of clinical fMRI data, mainly because of larger interpretational demands than for data processed using the model based GLM framework. However, data driven methods can potentially provide additional information in clinical fMRI experiments, such as information about several functional areas extracted from a single experiment. In Paper III, it was demonstrated that the proposed LLE algorithm for dimensionality reduction was capable of separating the fMRI data into spatial component maps capturing task-evoked activation as well as motion related activation. The performance of LLE compared well to the normally used PCA algorithm, and in a data set with simulated delay of HRF onset, LLE was able to identify activated voxels, whereas PCA and non-linear PCA failed in doing so. The algorithm was thus proposed as a

preprocessing step to ICA, with potential advantages in cases when the HRF is varying.

Recently, considerable interest has been shown in the possible diagnostic value of the resting state network, and measurements of resting state activation is potentially of great value in patient groups presently excluded from conventional fMRI, for example, children or severely impaired patients unable to cooperate during a classic task based experiment. In the study reported in Paper IV, the resting state motor network activation was found to be comparable to task evoked activation in terms of test-retest reproducibility. Further investigations are, however, needed in order to establish the validity of this method on an individual patient basis.

Acknowledgements

This thesis would not have been possible without the help from many people. In particular, I would like to express my gratitude to the following:

- My supervisor, Dr Johan Olsrud, for his extraordinary kindness, scientific skill and encouragement at all times.

- My co-supervisor, Professor Freddy Ståhlberg, for friendship, support, and for always finding a way forward.

- My other co-supervisor, Professor Ronnie Wirestam, for friendship, inspiring discussions and scientific support.

- My co-authors, Danielle van Westen, Anthony Waites, Marnie Shaw, Graeme Jackson, Henrik Hansson, Peter Fransson, Andreas Weibull and Jonas Svensson for rewarding scientific collaboration, and, especially Markus Nilsson for his extraordinary support.

- Present and past members of the MR physics group for pleasant company and friendship: Jimmy Lätt, Karin Markenroth, Linda Knutsson, Anders Nilsson, Adnan Bibic, Anna Rydhög, Emelie Lindgren, Johanna Mårtensson, Renata Madru, Sara Brockstedt, Edvin Johansson, Jacob Eberhardt and Oliver Thilmann

- Friends and colleagues at the MR Department, Skåne University Hospital, Lund, and at the Department for Medical Radiation Physics, Lund University, for friendship and for providing a wonderful working atmosphere.

- My parents, Ralf and Brigitte, for never-ending support.

- My family, Helena, Emma and Lukas, for their love and patience.

References

1. Roy CS, Sherrington CS. On the Regulation of the Blood-supply of the Brain. J Physiol 1890;11(1-2):85-158 117.
2. Pauling L, Coryell CD. The Magnetic Properties and Structure of Hemoglobin, Oxyhemoglobin and Carbonmonoxyhemoglobin. Proc Natl Acad Sci U S A 1936;22(4):210-216.
3. Thulborn KR, Waterton JC, Matthews PM, Radda GK. Oxygenation dependence of the transverse relaxation time of water protons in whole blood at high field. Biochim Biophys Acta 1982;714(2):265-270.
4. Ogawa S, Lee TM, Kay AR, Tank DW. Brain magnetic resonance imaging with contrast dependent on blood oxygenation. Proc Natl Acad Sci USA 1990;87(24):9868-9872.
5. Ogawa S, Lee T-M, Nayak AS, Glynn P. Oxygenation-sensitive contrast in magnetic resonance image of rodent brain at high magnetic fields. Magn Reson Med 1990;14(1):68.
6. Bandettini PA, Wong EC, Hinks RS, Tikofsky RS, Hyde JS. Time course EPI of human brain function during task activation. Magn Reson Med 1992;25(2):390-397.
7. Frahm J, Bruhn H, Merboldt KD, Hanicke W. Dynamic MR imaging of human brain oxygenation during rest and photic stimulation. J Magn Reson Imaging 1992;2(5):501-505.
8. Kwong KK, Belliveau JW, Chesler DA, Goldberg IE, Weisskoff RM, Poncelet BP, Kennedy DN, Hoppel BE, Cohen MS, Turner R, et al. Dynamic magnetic resonance imaging of human brain activity during primary sensory stimulation. Proc Natl Acad Sci U S A 1992;89(12):5675-5679.
9. Ogawa S, Tank DW, Menon R, Ellermann JM, Kim SG, Merkle H, Ugurbil K. Intrinsic signal changes accompanying sensory stimulation: functional brain mapping with magnetic resonance imaging. Proc Natl Acad Sci USA 1992;89(13):5951-5955.
10. Turner R, Le Bihan D, Moonen CT, Despres D, Frank J. Echo-planar time course MRI of cat brain oxygenation changes. Magn Reson Med 1991;22(1):159-166.

11. Aguirre GK, Detre JA, Alsop DC, D'Esposito M. The parahippocampus subserves topographical learning in man. Cereb Cortex 1996;6(6):823-829.

12. Binder JR, Swanson SJ, Hammeke TA, Morris GL, Mueller WM, Fischer M, Benbadis S, Frost JA, Rao SM, Haughton VM. Determination of language dominance using functional MRI: a comparison with the Wada test. Neurology 1996;46(4):978-984.

13. Karni A, Meyer G, Rey-Hipolito C, Jezzard P, Adams MM, Turner R, Ungerleider LG. The acquisition of skilled motor performance: fast and slow experience-driven changes in primary motor cortex. Proc Natl Acad Sci U S A 1998;95(3):861-868.

14. Kastner S, De Weerd P, Desimone R, Ungerleider LG. Mechanisms of directed attention in the human extrastriate cortex as revealed by functional MRI. Science 1998;282(5386):108-111.

15. Biswal B, Yetkin FZ, Haughton VM, Hyde JS. Functional connectivity in the motor cortex of resting human brain using echo-planar MRI. Magn Reson Med 1995;34(4):537-541.

16. Fox MD, Raichle ME. Spontaneous fluctuations in brain activity observed with functional magnetic resonance imaging. Nat Rev Neurosci 2007;8(9):700-711.

17. Gaillard WD, Bookheimer SY, Cohen M. The use of fMRI in neocortical epilepsy. Adv Neurol 2000;84:391-404.

18. Hirsch J, Ruge MI, Kim KH, Correa DD, Victor JD, Relkin NR, Labar DR, Krol G, Bilsky MH, Souweidane MM, DeAngelis LM, Gutin PH. An integrated functional magnetic resonance imaging procedure for preoperative mapping of cortical areas associated with tactile, motor, language, and visual functions. Neurosurgery 2000;47(3):711-721; discussion 721-712.

19. Lee CC, Ward HA, Sharbrough FW, Meyer FB, Marsh WR, Raffel C, So EL, Cascino GD, Shin C, Xu Y, Riederer SJ, Jack CR, Jr. Assessment of functional MR imaging in neurosurgical planning. AJNR Am J Neuroradiol 1999;20(8):1511-1519.

20. Stippich C. Clinical Functional MRI, Presurgical Functional Neuroimaging. Baert AL, Brady LW, Heilmann H-P, Knauth M, Molls M, Nider C, Sartor K, editors. Berlin, Heidelberg, New York: Springer-Verlag; 2007.

21. Stippich C, Kress B, Ochmann H, Tronnier V, Sartor K. [Preoperative functional magnetic resonance tomography (FMRI) in patients with rolandic brain tumors: indication, investigation strategy, possibilities and limitations of clinical application]. Rofo 2003;175(8):1042-1050.

22. Sunaert S. Presurgical planning for tumor resectioning. J Magn Reson Imaging 2006;23(6):887-905.

23. Sunaert S, Yousry TA. Clinical applications of functional magnetic resonance imaging. Neuroimaging Clin N Am 2001;11(2):221-236, viii.

24. Penfield W, Boldrey E. Somatic motor and sensory representation in the cerebral cortex of man as studied by electrical stimulation. Brain 1937;60(4):389-443.

25. Wada J, Rasmussen T. Intracarotid injection of sodium amytal for the lateralization of cerebral speech dominance. J Neurosurg 1960;106(6):1117-1133.

26. Fox PT, Raichle ME. Focal physiological uncoupling of cerebral blood flow and oxidative metabolism during somatosensory stimulation in human subjects. Proc Natl Acad Sci U S A 1986;83(4):1140-1144.

27. Fox PT, Raichle ME, Mintun MA, Dence C. Nonoxidative glucose consumption during focal physiologic neural activity. Science 1988;241(4864):462-464.

28. Menon RS, Ogawa S, Hu X, Strupp JP, Anderson P, Ugurbil K. BOLD based functional MRI at 4 Tesla includes a capillary bed contribution: echo-planar imaging correlates with previous optical imaging using intrinsic signals. Magn Reson Med 1995;33(3):453-459.

29. Davis TL, Weisskoff RM, Kwong KK, Boxerman JL, Rosen BR. Temporal aspects of fMRI task activation: dynamic modeling of oxygen delivery. Int Soc Magn Reson 2nd Annu Mtg 1994; San Francisco. p 69.

30. Malonek D, Grinvald A. Interactions between electrical activity and cortical microcirculation revealed by imaging spectroscopy: implications for functional brain mapping. Science 1996;272(5261):551-554.

31. Buxton RB, Wong EC, Frank LR. Dynamics of blood flow and oxygenation changes during brain activation: the balloon model. Magn Reson Med 1998;39(6):855-864.

32. Burock MA, Buckner RL, Woldorff MG, Rosen BR, Dale AM. Randomized event-related experimental designs allow for extremely rapid presentation rates using functional MRI. Neuroreport 1998;9(16):3735-3739.

33. Hoge RD, Atkinson J, Gill B, Crelier GR, Marrett S, Pike GB. Stimulus-dependent BOLD and perfusion dynamics in human V1. Neuroimage 1999;9(6 Pt 1):573-585.

34. Bonakdarpour B, Parrish TB, Thompson CK. Hemodynamic response function in patients with stroke-induced aphasia: implications for fMRI data analysis. Neuroimage 2007;36(2):322-331.

35. Peck KK, Bradbury MS, Hou BL, Brennan NP, Holodny AI. The role of the Supplementary Motor Area (SMA) in the execution of primary motor activities in brain tumor patients: functional MRI detection of time-resolved differences in the hemodynamic response. Med Sci Monit 2009;15(4):MT55-62.

36. Haase A, Frahm J, Matthaei D, Hanicke W, Merboldt KD. FLASH imaging. Rapid NMR imaging using low flip-angle pulses. J Magn Reson Resonance (1969) 1986;67(2):258.

37. Constable RT, McCarthy G, Allison T, Anderson AW, Gore JC. Functional brain imaging at 1.5 T using conventional gradient echo MR imaging techniques. Magn Reson Imaging 1993;11(4):451-459.

38. Schneider W, Noll DC, Cohen JD. Functional topographic mapping of the cortical ribbon in human vision with conventional MRI scanners. Nature 1993;365(6442):150.

39. Menon RS, Ogawa S, Tank DW, Ugurbil K. 4 Tesla gradient recalled echo characteristics of photic stimulation-induced signal changes in the human primary visual cortex. Magn Reson Med 1993;30(3):380-386.

40. Mansfield P. Multi-planar image formation using NMR spin echoes. J Phys C Solid State Physics 1977;10(3):L55.

41. Johnson G, Hutchison JMS, Redpath TW, Eastwood LM. Improvements in performance time for simultaneous three-dimensional NMR imaging. J Magn Reson (1969) 1983;54(3):374.

42. Belliveau JW, Kennedy DN, Jr., McKinstry RC, Buchbinder BR, Weisskoff RM, Cohen MS, Vevea JM, Brady TJ, Rosen BR. Functional mapping of the human visual cortex by magnetic resonance imaging. Science 1991;254(5032):716-719.

43. Noll DC, Cohen JD, Meyer CH, Schneider W. Spiral K-space MR imaging of cortical activation. J Magn Reson Imaging 1995;5(1):49-56.

44. Howseman AM, Grootoonk S, Porter DA, Ramdeen J, Holmes AP, Turner R. The effect of slice order and thickness on fMRI activation data using multislice echo-planar imaging. Neuroimage 1999;9(4):363-376.

45. Jezzard P, Balaban RS. Correction for geometric distortion in echo planar images from B0 field variations. Magn Reson Med 1995;34(1):65-73.

46. Pruessmann KP, Weiger M, Scheidegger MB, Boesiger P. SENSE: sensitivity encoding for fast MRI. Magn Reson Med 1999;42(5):952-962.

47. Sodickson DK, Manning WJ. Simultaneous acquisition of spatial harmonics (SMASH): fast imaging with radiofrequency coil arrays. Magn Reson Med 1997;38(4):591-603.

48. Bruder H, Fischer H, Reinfelder HE, Schmitt F. Image reconstruction for echo planar imaging with nonequidistant k-space sampling. Magn Reson Med 1992;23(2):311-323.

49. Buonocore MH, Gao L. Ghost artifact reduction for echo planar imaging using image phase correction. Magn Reson Med 1997;38(1):89-100.

50. Ehman RL, Felmlee JP. Adaptive technique for high-definition MR imaging of moving structures. Radiology 1989;173(1):255-263.

51. Devlin JT, Russell RP, Davis MH, Price CJ, Wilson J, Moss HE, Matthews PM, Tyler LK. Susceptibility-induced loss of signal: comparing PET and fMRI on a semantic task. Neuroimage 2000;11(6 Pt 1):589-600.

52. Reichenbach JR, Venkatesan R, Yablonskiy DA, Thompson MR, Lai S, Haacke EM. Theory and application of static field inhomogeneity effects in gradient-echo imaging. J Magn Reson Imaging 1997;7(2):266-279.

53. Fransson P, Merboldt KD, Ingvar M, Petersson KM, Frahm J. Functional MRI with reduced susceptibility artifact: high-resolution mapping of episodic memory encoding. Neuroreport 2001;12(7):1415-1420.

54. Powell HW, Richardson MP, Symms MR, Boulby PA, Thompson PJ, Duncan JS, Koepp MJ. Preoperative fMRI predicts memory decline following anterior temporal lobe resection. J Neurol Neurosurg Psychiatry 2008;79(6):686-693.

55. Rabin ML, Narayan VM, Kimberg DY, Casasanto DJ, Glosser G, Tracy JI, French JA, Sperling MR, Detre JA. Functional MRI predicts post-surgical memory following temporal lobectomy. Brain 2004;127(Pt 10):2286-2298.

56. Richardson MP, Strange BA, Thompson PJ, Baxendale SA, Duncan JS, Dolan RJ. Pre-operative verbal memory fMRI predicts post-operative memory decline after left temporal lobe resection. Brain 2004;127(Pt 11):2419-2426.

57. Deichmann R, Josephs O, Hutton C, Corfield DR, Turner R. Compensation of susceptibility-induced BOLD sensitivity losses in echo-planar fMRI imaging. Neuroimage 2002;15(1):120-135.

58. Lipschutz B, Friston KJ, Ashburner J, Turner R, Price CJ. Assessing study-specific regional variations in fMRI signal. Neuroimage 2001;13(2):392-398.

59. Gati JS, Menon RS, Ugurbil K, Rutt BK. Experimental determination of the BOLD field strength dependence in vessels and tissue. Magn Reson Med 1997;38(2):296-302.

60. Cusack R, Russell B, Cox SM, De Panfilis C, Schwarzbauer C, Ansorge R. An evaluation of the use of passive shimming to improve frontal sensitivity in fMRI. Neuroimage 2005;24(1):82-91.

61. Deichmann R, Gottfried JA, Hutton C, Turner R. Optimized EPI for fMRI studies of the orbitofrontal cortex. Neuroimage 2003;19(2 Pt 1):430-441.

62. Weiskopf N, Hutton C, Josephs O, Turner R, Deichmann R. Optimized EPI for fMRI studies of the orbitofrontal cortex: compensation of susceptibility-induced gradients in the readout direction. Magn Reson Mater Phy 2007;20(1):39-49.

63. Ojemann JG, Akbudak E, Snyder AZ, McKinstry RC, Raichle ME, Conturo TE. Anatomic localization and quantitative analysis of gradient refocused echo-planar fMRI susceptibility artifacts. Neuroimage 1997;6(3):156-167.

64. Weiskopf N, Hutton C, Josephs O, Deichmann R. Optimal EPI parameters for reduction of susceptibility-induced BOLD sensitivity losses: a whole-brain analysis at 3 T and 1.5 T. Neuroimage 2006;33(2):493-504.

65. Andersson JL, Hutton C, Ashburner J, Turner R, Friston K. Modeling geometric deformations in EPI time series. Neuroimage 2001;13(5):903-919.

66. Seto E, Sela G, McIlroy WE, Black SE, Staines WR, Bronskill MJ, McIntosh AR, Graham SJ. Quantifying head motion associated with motor tasks used in fMRI. Neuroimage 2001;14(2):284-297.

67. Hill DL, Smith AD, Simmons A, Maurer CR, Jr., Cox TC, Elwes R, Brammer M, Hawkes DJ, Polkey CE. Sources of error in comparing functional magnetic resonance imaging and invasive electrophysiological recordings. J Neurosurg 2000;93(2):214-223.

68. Wilson JL, Jezzard P. Utilization of an intra-oral diamagnetic passive shim in functional MRI of the inferior frontal cortex. Magn Reson Med 2003;50(5):1089-1094.

69. Cho ZH, Ro YM. Reduction of susceptibility artifact in gradient-echo imaging. Magn Reson Med 1992;23(1):193-200.

70. Stenger VA, Boada FE, Noll DC. Three-dimensional tailored RF pulses for the reduction of susceptibility artifacts in T(*)(2)-weighted functional MRI. Magn Reson Med 2000;44(4):525-531.

71. Constable RT, Spencer DD. Composite image formation in z-shimmed functional MR imaging. Magn Reson Med 1999;42(1):110-117.

72. Frahm J, Merboldt KD, Hanicke W. Direct FLASH MR imaging of magnetic field inhomogeneities by gradient compensation. Magn Reson Med 1988;6(4):474-480.

73. Glover GH. 3D z-shim method for reduction of susceptibility effects in BOLD fMRI. Magn Reson Med 1999;42(2):290-299.

74. Ordidge RJ, Gorell JM, Deniau JC, Knight RA, Helpern JA. Assessment of relative brain iron concentrations using T2-weighted and T2*-weighted MRI at 3 Tesla. Magn Reson Med 1994;32(3):335-341.

75. Frahm J, Merboldt KD, Hanicke W. Functional MRI of human brain activation at high spatial resolution. Magn Reson Med 1993;29(1):139-144.

76. Young IR, Cox IJ, Bryant DJ, Bydder GM. The benefits of increasing spatial resolution as a means of reducing artifacts due to field inhomogeneities. Magn Reson Imaging 1988;6(5):585-590.

77. Friston KJ, Williams S, Howard R, Frackowiak RS, Turner R. Movement-related effects in fMRI time-series. Magn Reson Med 1996;35(3):346-355.

78. Bullmore ET, Brammer MJ, Rabe-Hesketh S, Curtis VA, Morris RG, Williams SC, Sharma T, McGuire PK. Methods for diagnosis and treatment of stimulus-correlated motion in generic brain activation studies using fMRI. Hum Brain Mapp 1999;7(1):38-48.

79. Friston KJ, Worsley KJ, Frackowiak RSJ, Mazziotta JC, Evans AC. Assessing the significance of focal activations using their spatial extent. Hum Brain Mapp 1993;1(3):210.

80. Maes F, Collignon A, Vandermeulen D, Marchal G, Suetens P. Multimodality image registration by maximization of mutual information. IEEE Trans Med Imaging 1997;16(2):187-198.

81. Viola P, Wells Iii WM. Alignment by Maximization of Mutual Information. Int J Comput Vision 1997;24(2):137.

82. Roche A, Malandain G, Pennec X, Ayache N. The Correlation Ratio as a New Similarity Measure for Multimodal Image Registration. Proc MICCAI 1998.

83. Ashburner J, Friston KJ. Nonlinear spatial normalization using basis functions. Hum Brain Mapp 1999;7(4):254-266.

84. Evans AC, Collins DL, Mills SR, Brown ED, Kelly RL, Peters TM. 3D statistical neuroanatomical models from 305 MRI volumes. 1993. p 1813-1817.

85. Talairach J, Tournoux P. Co-planar stereotaxic atlas of the human brain. New York: Thieme Medical Publisher Inc.; 1988.

86. Friston KJ, Holmes AP, Worsley KJ, Poline JP, Frith CD, Frackowiak RSJ. Statistical parametric maps in functional imaging: A general linear approach. Hum Brain Mapp 1994;2(4):189.

87. Friston KJ, Jezzard P, Turner R. Analysis of functional MRI time-series. Hum Brain Mapp 1994;1(2):153.

88. Boynton GM, Engel SA, Glover GH, Heeger DJ. Linear systems analysis of functional magnetic resonance imaging in human V1. J Neurosci 1996;16(13):4207-4221.

89. Friston KJ, Fletcher P, Josephs O, Holmes A, Rugg MD, Turner R. Event-related fMRI: characterizing differential responses. Neuroimage 1998;7(1):30-40.

90. Worsley KJ, Evans AC, Marrett S, Neelin P. A three-dimensional statistical analysis for CBF activation studies in human brain. J Cereb Blood Flow Metab 1992;12(6):900-918.

91. Genovese CR, Lazar NA, Nichols T. Thresholding of statistical maps in functional neuroimaging using the false discovery rate. Neuroimage 2002;15(4):870-878.

92. Comon P. Independent component analysis, a new concept? Signal Process 1994;36(3):287-314.

93. Jutten C, Herault J. Blind separation of sources, Part 1: an adaptive algorithm based on neuromimetic architecture. Signal Process 1991;24(1):1-10.

94. McKeown MJ, Makeig S, Brown GG, Jung TP, Kindermann SS, Bell AJ, Sejnowski TJ. Analysis of fMRI data by blind separation into independent spatial components. Hum Brain Mapp 1998;6(3):160-188.

95. Hyvärinen A. Fast and Robust Fixed-Point Algorithms for Independent Component Analysis. IEEE T Neural Networ 1999;10(3):626.

96. Hyvärinen A, Oja E. A fast fixed-point algorithm for independent component analysis. Neural Comput 1997;9(7):1483-1492.

97. Bell AJ, Sejnowski TJ. An information-maximization approach to blind separation and blind deconvolution. Neural Comput 1995;7(6):1129-1159.

98. Lund TE, Norgaard MD, Rostrup E, Rowe JB, Paulson OB. Motion or activity: their role in intra- and inter-subject variation in fMRI. Neuroimage 2005;26(3):960-964.

99. Friston K, Phillips J, Chawla D, Buchel C. Nonlinear PCA: characterizing interactions between modes of brain activity. Philos Trans R Soc Lond B Biol Sci 2000;355(1393):135-146.

100. McKeown MJ, Sejnowski TJ. Independent component analysis of fMRI data: examining the assumptions. Hum Brain Mapp 1998;6(5-6):368-372.

101. Thirion B, Faugeras O. Nonlinear dimension Reduction of fMRI Data: The Laplacian Embedding Approach. 2004; Arlington, VA. p 372-375.

102. Shen X, Meyer FG. Low-dimensional embedding of fMRI datasets. Neuroimage 2008;41(3):886-902.

103. Roweis ST, Saul LK. Nonlinear dimensionality reduction by locally linear embedding. Science 2000;290(5500):2323-2326.

104. Tenenbaum JB, Silva Vd, Langford JC. A Global Geometric Framework for Nonlinear Dimensionality Reduction. Science 2000;290(5500):2319-2323.

105. Cox T, Cox M. Multidimensional Scaling. London, UK: Chapman & Hall; 1994.

106. Belkin M, Niyogi P. Laplacian eigenmaps and spectral techniques for embedding and clustering. 2002. p 585.

107. Raichle ME, Mintun MA. Brain work and brain imaging. Annu Rev Neurosci 2006;29:449-476.

108. Cordes D, Haughton VM, Arfanakis K, Wendt GJ, Turski PA, Moritz CH, Quigley MA, Meyerand ME. Mapping functionally related regions of brain with functional connectivity MR imaging. AJNR Am J Neuroradiol 2000;21(9):1636-1644.

109. De Luca M, Smith S, De Stefano N, Federico A, Matthews PM. Blood oxygenation level dependent contrast resting state networks are relevant to functional activity in the neocortical sensorimotor system. Exp Brain Res 2005;167(4):587-594.

110. Fox MD, Snyder AZ, Zacks JM, Raichle ME. Coherent spontaneous activity accounts for trial-to-trial variability in human evoked brain responses. Nat Neurosci 2006;9(1):23-25.

111. Lowe MJ, Mock BJ, Sorenson JA. Functional connectivity in single and multislice echoplanar imaging using resting-state fluctuations. Neuroimage 1998;7(2):119-132.

112. Xiong J, Parsons LM, Gao JH, Fox PT. Interregional connectivity to primary motor cortex revealed using MRI resting state images. Hum Brain Mapp 1999;8(2-3):151-156.

113. Cordes D, Haughton VM, Arfanakis K, Carew JD, Turski PA, Moritz CH, Quigley MA, Meyerand ME. Frequencies contributing to functional connectivity in the cerebral cortex in "resting-state" data. AJNR Am J Neuroradiol 2001;22(7):1326-1333.

114. Birn RM, Diamond JB, Smith MA, Bandettini PA. Separating respiratory-variation-related fluctuations from neuronal-activity-related fluctuations in fMRI. Neuroimage 2006;31(4):1536-1548.

115. Fox MD, Snyder AZ, Vincent JL, Corbetta M, Van Essen DC, Raichle ME. The human brain is intrinsically organized into dynamic, anticorrelated functional networks. Proc Natl Acad Sci U S A 2005;102(27):9673-9678.

116. Rombouts SA, Stam CJ, Kuijer JP, Scheltens P, Barkhof F. Identifying confounds to increase specificity during a "no task condition". Evidence for hippocampal connectivity using fMRI. Neuroimage 2003;20(2):1236-1245.

117. Macey PM, Macey KE, Kumar R, Harper RM. A method for removal of global effects from fMRI time series. Neuroimage 2004;22(1):360-366.

118. Zarahn E, Aguirre GK, D'Esposito M. Empirical analyses of BOLD fMRI statistics. I. Spatially unsmoothed data collected under null-hypothesis conditions. Neuroimage 1997;5(3):179-197.

119. De Martino F, Gentile F, Esposito F, Balsi M, Di Salle F, Goebel R, Formisano E. Classification of fMRI independent components using IC-fingerprints and support vector machine classifiers. Neuroimage 2007;34(1):177-194.

120. Buckner RL, Andrews-Hanna JR, Schacter DL. The brain's default network: anatomy, function, and relevance to disease. Ann N Y Acad Sci 2008;1124:1-38.

121. Fukunaga M, Horovitz SG, de Zwart JA, van Gelderen P, Balkin TJ, Braun AR, Duyn JH. Metabolic origin of BOLD signal fluctuations in the absence of stimuli. J Cereb Blood Flow Metab 2008;28(7):1377-1387.

122. Fukunaga M, Horovitz SG, van Gelderen P, de Zwart JA, Jansma JM, Ikonomidou VN, Chu R, Deckers RH, Leopold DA, Duyn JH. Large-amplitude, spatially correlated fluctuations in BOLD fMRI signals during extended rest and early sleep stages. Magn Reson Imaging 2006;24(8):979-992.

123. Horovitz SG, Braun AR, Carr WS, Picchioni D, Balkin TJ, Fukunaga M, Duyn JH. Decoupling of the brain's default mode network during deep sleep. Proc Natl Acad Sci USA 2009;106(27):11376-11381.

124. Horovitz SG, Fukunaga M, de Zwart JA, van Gelderen P, Fulton SC, Balkin TJ, Duyn JH. Low frequency BOLD fluctuations during resting wakefulness and light sleep: a simultaneous EEG-fMRI study. Hum Brain Mapp 2008;29(6):671-682.

125. Larson-Prior LJ, Zempel JM, Nolan TS, Prior FW, Snyder AZ, Raichle ME. Cortical network functional connectivity in the descent to sleep. Proc Natl Acad Sci U S A 2009;106(11):4489-4494.

126. Greicius MD, Kiviniemi V, Tervonen O, Vainionpaa V, Alahuhta S, Reiss AL, Menon V. Persistent default-mode network connectivity during light sedation. Hum Brain Mapp 2008;29(7):839-847.

127. Vincent JL, Patel GH, Fox MD, Snyder AZ, Baker JT, Van Essen DC, Zempel JM, Snyder LH, Corbetta M, Raichle ME. Intrinsic functional architecture in the anaesthetized monkey brain. Nature 2007;447(7140):83-86.

128. Fransson P, Aden U, Blennow M, Lagercrantz H. The Functional Architecture of the Infant Brain as Revealed by Resting-State fMRI. Cereb Cortex 2010.

129. Fransson P, Skiold B, Engstrom M, Hallberg B, Mosskin M, Aden U, Lagercrantz H, Blennow M. Spontaneous brain activity in the newborn brain during natural sleep--an fMRI study in infants born at full term. Pediatr Res 2009;66(3):301-305.

130. Fransson P, Skiold B, Horsch S, Nordell A, Blennow M, Lagercrantz H, Aden U. Resting-state networks in the infant brain. Proc Natl Acad Sci U S A 2007;104(39):15531-15536.

131. Greicius MD, Srivastava G, Reiss AL, Menon V. Default-mode network activity distinguishes Alzheimer's disease from healthy aging: evidence from functional MRI. Proc Natl Acad Sci U S A 2004;101(13):4637-4642.

132. Wang K, Jiang T, Liang M, Wang L, Tian L, Zhang X, Li K, Liu Z. Discriminative analysis of early Alzheimer's disease based on two intrinsically anti-correlated networks with resting-state fMRI. Med Image Comput Comput Assist Interv 2006;9(Pt 2):340-347.

133. Wang K, Liang M, Wang L, Tian L, Zhang X, Li K, Jiang T. Altered functional connectivity in early Alzheimer's disease: a resting-state fMRI study. Hum Brain Mapp 2007;28(10):967-978.

134. Wang L, Zang Y, He Y, Liang M, Zhang X, Tian L, Wu T, Jiang T, Li K. Changes in hippocampal connectivity in the early stages of Alzheimer's disease: evidence from resting state fMRI. Neuroimage 2006;31(2):496-504.

135. Lowe MJ, Beall EB, Sakaie KE, Koenig KA, Stone L, Marrie RA, Phillips MD. Resting state sensorimotor functional connectivity in multiple sclerosis inversely correlates with transcallosal motor pathway transverse diffusivity. Hum Brain Mapp 2008;29(7):818-827.

136. Lowe MJ, Phillips MD, Lurito JT, Mattson D, Dzemidzic M, Mathews VP. Multiple sclerosis: low-frequency temporal blood oxygen level-dependent fluctuations indicate reduced functional connectivity initial results. Radiology 2002;224(1):184-192.

137. Anand A, Li Y, Wang Y, Wu J, Gao S, Bukhari L, Mathews VP, Kalnin A, Lowe MJ. Activity and connectivity of brain mood regulating circuit in depression: a functional magnetic resonance study. Biol Psychiatry 2005;57(10):1079-1088.

138. Anand A, Li Y, Wang Y, Wu J, Gao S, Bukhari L, Mathews VP, Kalnin A, Lowe MJ. Antidepressant effect on connectivity of the mood-regulating circuit: an FMRI study. Neuropsychopharmacol 2005;30(7):1334-1344.

139. Greicius MD, Flores BH, Menon V, Glover GH, Solvason HB, Kenna H, Reiss AL, Schatzberg AF. Resting-state functional connectivity in major depression: abnormally increased contributions from subgenual cingulate cortex and thalamus. Biol Psychiatry 2007;62(5):429-437.

140. Bluhm RL, Miller J, Lanius RA, Osuch EA, Boksman K, Neufeld RW, Theberge J, Schaefer B, Williamson P. Spontaneous low-frequency fluctuations in the BOLD signal in schizophrenic patients: anomalies in the default network. Schizophr Bull 2007;33(4):1004-1012.

141. Liang M, Zhou Y, Jiang T, Liu Z, Tian L, Liu H, Hao Y. Widespread functional disconnectivity in schizophrenia with resting-state functional magnetic resonance imaging. Neuroreport 2006;17(2):209-213.

142. Liu H, Liu Z, Liang M, Hao Y, Tan L, Kuang F, Yi Y, Xu L, Jiang T. Decreased regional homogeneity in schizophrenia: a resting state functional magnetic resonance imaging study. Neuroreport 2006;17(1):19-22.

143. Zhou Y, Liang M, Jiang T, Tian L, Liu Y, Liu Z, Liu H, Kuang F. Functional dysconnectivity of the dorsolateral prefrontal cortex in first-episode schizophrenia using resting-state fMRI. Neurosci Lett 2007;417(3):297-302.

144. Waites AB, Briellmann RS, Saling MM, Abbott DF, Jackson GD. Functional connectivity networks are disrupted in left temporal lobe epilepsy. Ann Neurol 2006;59(2):335-343.

145. Cao Q, Zang Y, Sun L, Sui M, Long X, Zou Q, Wang Y. Abnormal neural activity in children with attention deficit hyperactivity disorder: a resting-state functional magnetic resonance imaging study. Neuroreport 2006;17(10):1033-1036.

146. Tian L, Jiang T, Wang Y, Zang Y, He Y, Liang M, Sui M, Cao Q, Hu S, Peng M, Zhuo Y. Altered resting-state functional connectivity patterns of anterior cingulate cortex in adolescents with attention deficit hyperactivity disorder. Neurosci Lett 2006;400(1-2):39-43.

147. Zang YF, He Y, Zhu CZ, Cao QJ, Sui MQ, Liang M, Tian LX, Jiang TZ, Wang YF. Altered baseline brain activity in children with ADHD revealed by resting-state functional MRI. Brain Dev 2007;29(2):83-91.

148. Chen EE, Small SL. Test-retest reliability in fMRI of language: group and task effects. Brain Lang 2007;102(2):176-185.

149. Shimony JS, Zhang D, Johnston JM, Fox MD, Roy A, Leuthardt EC. Resting-state spontaneous fluctuations in brain activity: a new paradigm for presurgical planning using fMRI. Acad Radiol 2009;16(5):578-583.

150. Chen S, Ross TJ, Zhan W, Myers CS, Chuang KS, Heishman SJ, Stein EA, Yang Y. Group independent component analysis reveals consistent resting-state networks across multiple sessions. Brain Res 2008;1239:141-151.

151. Van Dijk KR, Hedden T, Venkataraman A, Evans KC, Lazar SW, Buckner RL. Intrinsic functional connectivity as a tool for human connectomics: theory, properties, and optimization. J Neurophysiol 2010;103(1):297-321.

152. Genovese CR, Noll DC, Eddy WF. Estimating test-retest reliability in functional MR imaging. I: Statistical methodology. Magn Reson Med 1997;38(3):497-507.

153. Noll DC, Genovese CR, Nystrom LE, Vazquez AL, Forman SD, Eddy WF, Cohen JD. Estimating test-retest reliability in functional MR imaging. II: Application to motor and cognitive activation studies. Magn Reson Med 1997;38(3):508-517.